Depth-dependent controls on structure, reactivation and geomorphology of the active Thyolo border fault, Malawi rift

Luke N. J. Wedmore[1], Jack N Williams[2], Juliet Biggs[1], Åke Fagereng[2], Felix Mphepo[3], Zuze Dulanya[4], James Willoughby[1], Hassan Mdala[3], Byron Adams[1]*

[1]School of Earth Sciences, University of Bristol, UK

[2]School of Earth and Ocean Sciences, Cardiff University, UK

[3]Geological Survey Department, Mzuzu Regional Office, Mzuzu, Malawi

[4]Geography and Earth Sciences Department, University of Malawi, Zomba, Malawi

**Corresponding author: luke.wedmore@bristol.ac.uk*

Depth-dependent controls on structure, reactivation and geomorphology of the active Thyolo border fault, Malawi rift

Luke N. J. Wedmore[1], Jack N Williams[2], Juliet Biggs[1], Åke Fagereng[2], Felix Mphepo[3], Zuze Dulanya[4], James Willoughby[1], Hassan Mdala[3], Byron Adams[1]*

[1]School of Earth Sciences, University of Bristol, UK

[2]School of Earth and Ocean Sciences, Cardiff University, UK

[3]Geological Survey Department, Mzuzu Regional Office, Mzuzu, Malawi

[4]Geography and Earth Sciences Department, University of Malawi, Zomba, Malawi

**Corresponding author: luke.wedmore@bristol.ac.uk*

Keywords

High-resolution topography, pre-existing structures, normal faults, rifts, border fault, damage zone

Highlights

- The Thyolo fault, Malawi, is a rift border fault with a polyphase tectonic history
- Satellite and field data confirm recent activity on an 18.6 ± 7.7 m high scarp
- The fault is segmented, but scarp height sectors do not align with geometry changes
- The fault damage zone is 15-180 m wide with an unusually narrow 0.7 m fault core
- The Thyolo fault may be reactivating a deep ductile zone along a terrane boundary

Abstract

We present new observations of the geometry and pattern of fault growth from the Thyolo fault, an 85 km long border fault in the southern Malawi Rift, from high-resolution topography and field observations. The rift has a polyphase tectonic history and the Thyolo fault is located towards the edge of the Proterozoic Unango Terrane. Recent activity is demonstrated by an 18.6 ± 7.7 m high fault scarp. Different patterns of segmentation are indicated by fault geometry and fault displacement profiles: two substantial reductions in scarp height do not coincide with surface geometry changes. The surface scarp is divided into two geometrically defined overlapping sections, which are joined by a ~5 km long, fault perpendicular scarp. The scarp height in this linking section is similar to the bounding sections, yet the river drainage network and sediment depocenter distribution is not typical of relay zones. Microstructural and compositional analyses show a 15-180 m thick damage zone with an unusually narrow 0.7 m thick fault core. These features can be explained if the fault exploits weak ductile zones at depth, such as heterogeneity associated with the Unango Terrane boundary, while near surface geometry is controlled by well-oriented, frictionally strong but low-cohesion shallow structures.

1. Introduction

Narrow amagmatic rifts (sensu Buck, 1991), are typically characterised by a ≤100 km wide graben or half graben where the greatest cumulative displacement is accommodated on large offset normal fault systems, known as rift border faults, that bound a region of distributed but relatively small displacement brittle deformation (Ebinger, 1989; Gawthorpe and Leeder, 2000; Muirhead et al., 2019). These basin-bounding faults are thought to be most active prior to any magmatic influence on rifting (Ebinger, 2005; Muirhead et al., 2019), have a distinctive impact on basin geomorphology (Leeder and Gawthorpe, 1987; Gawthorpe and Leeder, 2000) and can accumulate sufficient displacement so that flexural bending induces intrabasin strain (Turcotte and Schubert, 2002). Furthermore, border faults can penetrate the entire depth of the crust, and in East Africa are probably the source of some of the deep earthquakes within the ~40 km thick seismogenic layer (Lavayssière et al., 2019).

How faults grow from nucleation to crustal scale features is a long-standing topic of research (Cowie and Scholz, 1992b; Cowie, 1998; Walsh et al., 2002; Nicol et al., 2005; Worthington and Walsh, 2017; Rotevatn et al., 2019), and numerous studies have mapped fault trace geometry and measured displacement-length profiles to discuss the mechanism and timing of how long faults develop through segment initiation, growth, and linkage (Cowie and Scholz, 1992a, 1992b, 1992c; Scholz et al., 1993; Dawers et al., 1993; Dawers and Anders, 1995; Schlische et al., 1996; Walsh et al., 2003; Nicol et al., 2005, 2017; Giba et al., 2012; Rotevatn et al., 2018). Structural heterogeneities at segment boundaries that result from fault growth are thought to influence the propagation and termination of earthquake ruptures (Segall and Pollard, 1980; Zhang et al., 1991; Wesnousky, 2006, 2008), yet recent earthquakes (e.g. 2010 M_w7.2 El Mayor-Cucapah Earthquake, Mexico – Wei et al., 2011 and the 2016 M_w7.8 Kaikoura Earthquake, New Zealand – Hamling et al., 2017) have cut across multiple segment boundaries and thus it remains unclear how to best assess fault segmentation for seismic hazard purposes (DuRoss et al., 2016). Border faults are now generally thought to develop through the accumulation of displacement on fault segments that formed and linked during the early stages of rifting (Gawthorpe et al., 2003; Rotevatn et al., 2019; Muirhead et al., 2019); however, the effects of this linkage on the displacement profile and geometry of a fault is commonly long-lasting. Minima in fault displacement profiles and displacement anomalies are persistently observed at segment boundaries (Machette et al., 1991; Gupta and Scholz, 2000; Mortimer et al., 2007, 2016) as are relay ramps, increased fault complexity, and changes in fault geometry (Leeder and Gawthorpe, 1987; Crone and Haller, 1991a; Peacock and Sanderson, 1991; Crider and Pollard, 1998; Fossen and Rotevatn, 2016; Hodge et al., 2018a). Thus, observations of fault segmentation provide a permanent record of processes that occurred during the formation and linkage of fault segments, and consequently they offer insights into the fundamental processes of fault growth and the controls on the limits of earthquake rupture propagation.

Rifts rarely initiate and grow in isotropic crust, and therefore it is important to understand the effect of pre-existing heterogeneities and structures on the growth and segmentation of faults. Structures, such as pre-existing lithospheric weaknesses, are often cited as the predominant control on rift geometry, the distribution of strain within rifts, and the oblique orientation of magmatic bodies, magmatic rift segments and faults relative to the regional minimum compressive stress (McConnell, 1967; Daly et al., 1989; Ebinger et al., 1997; Morley, 2010; Henstra et al., 2015; Robertson et al., 2016; Muirhead and Kattenhorn, 2018). At the scale of an individual fault, the effect of pre-existing fabrics on fault growth has been constrained using analogue models, where reactivated structures have been shown to affect the fault geometry, relay zone geometry and the distribution of basins (Bellahsen and Daniel, 2005; Henza et al., 2011). However, comparisons with real faults in a natural setting is often more difficult as it can be difficult to differentiate between contemporary and pre-rift heterogeneities that have similar geometries (Smith and Mosley, 1993; Holdsworth et al., 1997), especially using seismic reflection and aeromagnetic surveys, which can only resolve features at scales >10 m.

Investigating the interactions between pre-existing fabrics and strain localisation on rift border faults also requires understanding the structure and mechanics of these faults. In general, as faults grow, they accumulate damage in the rocks surrounding the fault (Cowie and Scholz, 1992b; Caine et al., 1996; Shipton and Cowie, 2003). However, the structure of a rift border fault has only been described in a limited number of cases (Ord et al., 1988; Wheeler and Karson, 1989; Kristensen et al., 2016; Hollinsworth et al., 2019), with most models of normal fault structural evolution based on studies of small displacement (<100 m) faults within high porosity sedimentary rock (Shipton and Cowie, 2003; Childs et al., 2009; Torabi and Berg, 2011; Savage and Brodsky, 2011). Consequently, it remains unclear whether these models are applicable to large offset rift border faults where the footwall is composed of foliated crystalline metamorphic rocks.

In this paper, we analyse the Thyolo fault, the border fault of the Lower Shire Graben in southern Malawi (Figure 1). The fault is an ideal location to study the effects of reactivation on fault geometry, structure and geomorphology as the graben has a well-documented polyphase history of extension (Castaing, 1991; Chisenga et al., 2019) and in the current rift phase, the syn-rift sediments are thin and fault exposures are not hidden by any post-rift sediments (e.g. Hodge et al., 2019; Williams et al., 2019). We begin by describing the tectonic history of the region, before analysing the current activity, geometry, structure and geomorphology of the fault. In doing so, we assess how reactivation of pre-existing fabrics and heterogeneities affect the evolution of a rift border fault and discuss implications for the tectonic geomorphology of reactivated basin-bounding faults.

2. Tectonic History

The Thyolo fault bounds the north-eastern edge of the Lower Shire graben, which is located at the southern end of the largely amagmatic Western branch of the East African Rift (EAR; Figure 1). Extension within the Western branch of the EAR initiated ~25 Ma (Roberts et al., 2012) and within southern Malawi, the extension rate is ~2 mm yr^{-1} (Stamps et al., 2018; Figure 1). The footwall of the Thyolo fault is composed of charnockitic gneiss and granitic granulites of the Mesoproterozoic Unango Terrane, part of the Mozambique Belt, with the fault located towards the southwestern edge of the terrane (Fullgraf et al. *in press*; Bloomfield, 1965; Johnson et al., 2005). The Unango Terrane likely formed in a continental volcanic arc setting at ~1 Ga, and experienced granulite facies metamorphism associated with ductile deformation shortly after emplacement (957 ± 27 Ma; Bingen et al., 2009). Within the footwall of the Thyolo fault, the present-day NW-SE striking metamorphic foliation and migmatitic banding was formed during granulite facies metamorphism and partial melting that occurred during a series of collisional events at a convergent continental margin in the Pan-African Orogeny (~710-555 Ma) and the associated amalgamation of Gondwana (Kröner et al., 2001; Johnson et al., 2005; Manda et al., 2019). In the region of the Thyolo fault, the edge of the Unango Terrane is in contact with the basement of the Southern Irumide Belt which underwent peak metamorphism between 1.06 and 1.05 Ga (Johnson et al., 2005; Westerhof et al., 2008; Karmakar and Schenk, 2016). The boundaries between terranes have been roughly mapped based on exposures within Malawi (Manda et al., 2019), but because Karoo sediment have obscured the basement, the unit boundaries are largely extrapolated from neighbouring Mozambique, where mapping was supported by geochemical and airborne magnetic data (Bingen et al., 2009; Macey et al., 2010).

2.1 Previous phases of rifting

The Lower Shire graben contains Phanerozoic sedimentary and volcanic deposits related to three regional phases of extension that occurred prior to the current rifting: two distinct events during the Karoo-age (~330-180 Ma) breakup of Gondwana, and a later phase during the Cretaceous (Castaing, 1991; Figure 2).

NW-SE Karoo-age extension in the Lower Shire Graben created space to deposit a sequence of Late Ecca (Middle Permian) to Late Beaufort (Early Triassic) coal shales, coarse grained grits, mudstones and sandstones (Figure 2c). These sedimentary deposits are bound by NE-SW striking normal faults and NW-SE striking dextral strike-slip faults including the Mwanza and possibly the Thyolo fault (Figure 2c; Habgood, 1963; Habgood et al., 1973; Castaing, 1991).

NW-SE extension continued into the late Karoo period, when it was associated with basaltic volcanism and contemporaneous emplacement of NE-SW striking dolerite dykes. These dykes and volcanic deposits are collectively known as the Stormberg Volcanics, which are widely observed in the footwalls of the Mwanza, Thyolo and Mtumba faults (Figure 2d; Habgood, 1963; Habgood et al., 1973; Woolley et al., 1979; Castaing, 1991).

At the end of the Karoo period (Late Jurassic – Cretaceous), the extension direction rotated from NW-SE to NE-SW and reactivated NW-SE transtensional structures established in the earlier phase of NW-SE extension as dip-slip normal faults (Figure 2e; Castaing, 1991). In the Lower Shire Graben, remnants from the NE-SW extension are limited to sandstones in the hanging wall of the Panga and Chitsumba faults (Figure 2e) and siliceous fault rock along the Namalambo Fault. These sedimentary deposits form part of the Lupata series, a mix of coarse grained sandstones, and rhyolitic and alkaline lavas found extensively in Mozambique (Dixey and Campbell Smith, 1929; Habgood, 1963), and emplaced contemporaneously with the Chilwa Alkaline Province, which involves intrusive rocks that crosscut the Stormberg dykes (Macdonald et al., 1983; Woolley, 1987; Castaing, 1991; Eby et al., 1995). Cretaceous activity on the Thyolo and/or Mwanza faults cannot be ruled out as any Cretaceous sedimentary deposits will likely have been buried by current syn-rift sediments.

2.2 Present day rifting

Some previous studies in the region have interpreted the Thyolo fault as a reactivated dextral strike-slip fault linking the Urema Graben (the southern active continuation of the EARS in Mozambique) and the Zomba Graben (Castaing, 1991; Chorowicz and Sorlien, 1992; Chorowicz, 2005). In other studies, the Thyolo fault is considered inactive (Laõ-Dávila et al., 2015; Prater et al., 2016). However, remote sensing observations have identified an active fault scarp along the Thyolo fault and triangular facets at the southern end of the fault, which demonstrate that the Thyolo fault is currently active (Hodge et al., 2019). A M_w5.6 earthquake in March 2018 had a normal faulting focal mechanism with nodal planes aligned with the surface traces of faults in the Lower Shire Graben (Figure 1). Williams et al. (2019) suggest that the Thyolo fault is currently active as a dip-slip normal fault oriented obliquely to the regional extension direction.

2.3 Summary

The Thyolo fault, that bounds the Lower Shire Graben, is hosted towards the edge of the Unango Terrane which underwent granulite facies metamorphism during continental collision and terrane accretion in Pan-African Orogeny resulting in a NW-SE oriented foliation. Since this time, the faults in the Lower Shire graben have been active during four distinct periods of horizontal extension. Two phases during the Karoo, a period of extension during the Cretaceous and the present phase of active rifting. Below, we describe in detail the dimensions and geometry of the fault scarp along the Thyolo fault, including factors that control fault segmentation and orientation, and analysis of the fault zone structure.

3. Fault Segmentation

3.1 Methods

We use a high resolution 12 m TanDEM-X digital elevation model (DEM) to identify different indicators of fault segmentation based on two distinct sets of criteria: map-view geometry and scarp height. Geometrical criteria for fault segmentation were identified by Zhang et al. (1991) as changes in fault strike, changes in fault width, fault branches, gaps and steps in map view. Broadly speaking, these areas of increased fault complexity are indicators of segment boundaries (DuRoss et al., 2016), and have been noted as a limiting factor for earthquake ruptures (Segall and Pollard, 1980), especially when gaps are greater than 3-5 km (Wesnousky, 2008). In this study we mapped the fault trace in high resolution and noted prominent changes in fault strike and fault steps that may be indicative of fault segmentation.

Fault segmentation can also be defined from the profile of scarp height (e.g. Dawers and Anders, 1995; Willemse et al., 1996; Willemse, 1997; Walsh et al., 2003). In a plot of displacement vs. fault-parallel distance, the segment boundaries are located at local minima in displacement (Crone and Haller, 1991a; Dawers and Anders, 1995; Walsh et al., 2003). We used the scarp height measurements as a proxy for displacement (e.g. Morewood and Roberts, 2000; Hodge et al., 2018b, 2019; Wedmore et al., 2019) to identify segments based on local minima in the along-strike scarp height profile. We use adapted versions of the SPARTA tools (Hodge et al., 2019) to measure the height of the fault scarp along the Thyolo fault on the 12 m DEM. We differ from Hodge et al., 2019 by extracting 500 m long fault-perpendicular topographic profiles from the DEM every 12 m along the fault, which are then stacked at 100 m intervals before measuring the vertical difference between regression lines on the footwall and hanging wall surfaces. We estimate the uncertainty of each measurement by applying a Monte Carlo approach to sample 10,000 random subsets of points from the hanging wall and footwall of the fault as well as allowing the location of the fault to vary along the section of the topographic profiles identified as the fault scarp. The resulting measurements of vertical offset were then filtered using a 5 km wide moving median filter along the strike of the fault.

We also examined the Thyolo fault for any evidence of features associated with fault linkage. Where two un-linked fault segments interact, structures form such that the faults maintain laterally constant extensional strain (Walsh and Watterson, 1991).

The relay or transfer structures evolve as the faults overlap and link to form a distinctive set of features, including 10-15° dipping ramps and breach structures that link the segments and are often twisted and rotated (about a vertical axis) by the tips of the overlapping, propagating faults prior to breaching (Fossen and Rotevatn, 2016). We analysed the strike of the fault by dividing the fault trace into 50 m long sections and measuring the strike of each section from the trend of the surface trace, assuming negligible topography. The orientation of pre-existing basement structures were also analysed by digitising the 3D foliation measurements and strike of dolerite (Stormberg) dykes in Habgood et al. (1973).

3.2 Results

During a field campaigns in 2017 and 2018, we observed a recent fault scarp at the base of the Thyolo fault's 1 km high footwall escarpment (Figure 1c). Hodge et al. (2019) then identified a pseudo-continuous scarp along two structures totalling 85 km in length, the Thyolo and Muona faults, using high-resolution topography data, but divided the fault into two separate faults. In the following sections, we consider the Thyolo and Muona faults as a singular fault rather than two separate structures, although we do differentiate between the Thyolo and Muona sections of the fault (Figure 3). Triangular facets are visible within the high resolution topography along the southeastern end of the Thyolo section and the northwestern end of the Muona section (Figure 3). We observed no systematic deflection of river channels or any other geomorphological features that might indicate strike-slip faulting, and we therefore consider the Thyolo fault to be currently accommodating pure normal dip-slip displacement (see also Williams et al., 2019). We used further field observations from 2018 to ground truth the geometrical and scarp height observations from high resolution topography and geological maps detailed in the following sections.

3.2.1 Map View Geometry

The Thyolo fault is ~85 km long and has a mean strike of 139 ± 15° (1 standard deviation) dipping to the south west (Figure 3 & 4). A fault scarp was visible in the high-resolution topography along the length of the fault, with gaps observed where major rivers cross the fault and have eroded the scarp (Figure 3b). High-resolution mapping of the scarp found seven sections along the fault which trend approximately perpendicular to the main fault (Figure 4c). These NE-SW oriented sections have a mean strike of 034 ± 8° (black lines in Figure 4) with five sections dipping to the northwest and two sections dipping to the southeast. The dip angle of these NE-SW oriented sections is unknown but is likely steep based on the slope of the facet in the escarpment above (Figure 5). The most prominent of these NE-SW sections forms a 4.8 km near orthogonal link between the Thyolo and Muona sections (Figure 5). The ~69 km long Thyolo and the ~28 km long Muona sections overlap by ~10 km and are separated by this 4.8 km long strike-perpendicular section, which we refer to as the Chisumbi section. The six other scarp sections that strike perpendicular to the main fault are each <500 m long.

The mean strike of the foliation within the footwall of the Thyolo fault is 140 ± 37° with a dip of 56 ± 12° to the SW (Figure 4 & 5). This is sub parallel to the mean strike of the fault scarp (139 ± 15°) and the dip of the fault (assuming Andersonian mechanics). Conversely, the mean strike of the dolerite dykes in the fault's footwall is 037 ± 9° which is the same (within error) as the strike-perpendicular sections of the fault (034 ± 8°; including the Chisumbi section). Our field measurements at four localities along the Thyolo Fault indicate that the dykes are vertically dipping (Figure 3a). Thus, the main sections of the Thyolo fault are sub-parallel to the metamorphic foliation and dip in the same direction. In addition, the foliation dips at an angle that is within the typical range of active normal fault dips (45°-60°; Collettini and Sibson, 2001; Figure 4). However, in places the fault trace crosscuts the foliation at a high angle and is instead subparallel to the surface trace of footwall dolerite dykes (Figure 5).

3.2.2 Scarp Height

The median height of the fault scarp along the Thyolo fault is 18.6 ± 7.7 m (calculated as the median of the 5 km moving median plotted in Figure 4). The along strike profile of the scarp height measurements shows two scarp height minima (besides the tips of the fault; Figure 4b). The distance from fault tip to the first minimum is 28 km with a median scarp height of 24.9 ± 9.0 m in this portion of fault (Figure 4b). The next portion of fault is 15 km long and has a median scarp height of 20.8 ± 6.3 m. The final portion is 48 km long with median scarp height of 17.8 ± 6.5 m (Figure 4b). None of the scarp height minima identified from the scarp height profile coincide with fault geometrical changes, i.e. the short segments that strike perpendicular to the main fault (Figure 4).

3.2.3 The Chisumbi Section

The 4.8 km Chisumbi sections links the Muona and Thyolo sections and is oriented at 105 ± 17° to the strike of the main fault but subparallel to the dolerite dykes (Figure 5). Along this linking section, we observed a 19.0 ± 4.2 m high scarp (profile

D in Figure 3b; Figure 4). This height (yellow triangle in Figure 4b) is within the error bounds of the scarps found along the adjacent Muona and Thyolo sections. Thus, the fault scarp along Chisumbi section has a similar height to the bounding sections that it is approximately perpendicular to.

One possibility is that the Chisumbi section is a breached relay ramp. However, the morphology of the Chisumbi section is subtly different from the typical form of relay ramps. To show this we compare structural features from the footwall of the Chisumbi section with both the bounding Muona and Thyolo sections and to the expected geometry of relay ramps from global examples. The dolerite dykes within the overlapping zone have a strike of 031 ± 9° whereas the strike of the dolerite dykes outside the overlap zone is 038 ± 9° (Figure 5b). Thus, as these values are within the error bounds of each other, the average trace of dykes within the overlapping zones have either no rotation or a slight anticlockwise rotation around a vertical axis (Figure 5b). A clockwise rotation would be expected for the overlapping geometry (Figure 9a), and therefore, the observations indicate little strain has been induced during the process of fault linkage. Furthermore, breaching of a relay ramp normally occurs when a 10-15° ramp has formed (Figure 9b), with distinctive morphologies depending on the location of the breach (Figure 9a; Fossen and Rotevatn, 2016). The dip of the topography (excluding the facet slope above the fault scarp) in this overlapping zone is 2° (Figure 5c), so the Chisumbi scarp is unlikely to a breached relay ramp.

The Chisumbi section has a unique geomorphological signature, unlike that seen in typical ramp geometries (Densmore et al., 2003). While river channels often bend around propagating fault tips to avoid impinging zones of high rock uplift rates, the river channels of the Thyolo run perpendicular to the fault trace and show few signs of bending in the footwall of the fault. An important exception to this is the Chizimbi River which flows to the northwest along the from the southern end of the Thyolo fault, and marks the northern extent of the Chisumbi section (Figure 9). Such a regional drainage network is not predicted by the lithospheric deformation associated with relay ramp formation or longer-term evolution (Densmore et al., 2003 and Figure 9a), and thus requires a different formation mechanisms. A further consequence of this unusual pattern of drainage is that alluvial fans located in the hanging wall of the inboard Thyolo section extend much further from the fault trace (~5km) than alluvial fans on the outboard Muona section (~2 km; see contours in Figure 5b). We discuss the origins of this structure further in section 5.1.

4. Damage zone and fault core structure of the Thyolo fault

4.1 Sample collection and analysis

The footwall damage zone of the Thyolo fault zone is exposed at four localities: Kalulu, Kanjedza, Mbewe, and Muona (Figure 3). At each exposure, we made lithological and structural observations along transects from the fault scarp to distances up to 280 m from the fault. In addition, samples were collected at Kalulu (n = 5) and Kanjedza (n = 11) respectively for microstructural and compositional analyses. To locate the samples relative to a line perpendicular to the fault’s orientation (139/60 SW), as well as to survey the fault scarp and footwall structures, we captured aerial photography using a DJI Phantom 3 drone with onboard GPS positioning. At Kalulu, images were captured in a regular grid with three different flight plans taking photos from a range of viewing angles and elevations using the software DJI Groundstation Pro. At Kanjedza and Mbewe, drone photography was augmented with images from a handheld Canon Powershot SX280 HS camera with inbuilt GPS. Digital elevation models and orthophotos were constructed from these images using the structure-from-motion technique within Agisoft Metashape Pro (Johnson et al., 2014). The three samples furthest from the fault at Kanjedza were outside the drone survey and on the escarpment itself. The locations of these samples were instead measured with a handheld GPS, and their distance from the Thyolo fault was measured based on the distance between the sample and the fault projected from its surface trace at a dip of 60° (see figure S1 in the supplementary material).

Thin sections were made of all samples for microstructural analysis and fracture density measurements. At both sites, the fault is roughly foliation parallel, and so by cutting samples along the foliation dip-direction, they can be approximated as being perpendicular to the fault plane. Some samples did not contain a discernible foliation; for these samples, thin sections were instead cut at random orientations. Note that differences in thin section orientation do not appear to influence our microfracture density measurements (Figure 8h).

To measure microfracture density (defined as fracture length per sample area in mm^{-1}), three 10-15 mm^2 sample areas were selected in each thin section. These were derived by photographing the area at 5x magnification in plane polarised light (PPL) and cross polarised light (XPL) under a petrographic microscope, and then stitching the photomicrographs together using the MosaicJ plugin in ImageJ. To minimise the influence of orientation bias in fracture density quantification (e.g. Terzaghi, 1965), each sample area had a square shape.

Fractures were traced based on interpretations of both the PPL and XPL images of the sample area at a constant 200% zoom. Only fractures within quartz or feldspar grains were traced, to allow comparison between lithologically diverse samples, and fractures whose centres were not in the sample area were removed to reduce censoring effects (Zeeb et al., 2013). Cleavage sets could be differentiated from fractures in feldspar grains as cleavages tended to be deflected by twinning or form intragranular systematic sets at 90° to each other (Figure 8b). The total length of fracture traces in each sample area was calculated using FracPaQ 2.2 (Healy et al., 2017). To determine fracture density, total fracture length was then divided by sample area, which was calculated after filtering regions in the image that constituted non-quartzofeldspathic grains, or missing areas of the thin section that had been lost during sample preparation. The fracture density for each thin section was then calculated from the area-weighted average of its three sample areas.

4.2 Observations

The contact between footwall gneisses and hanging-wall sediments is exposed at Kalulu (Figure 6). These two units are separated by a 0.7 m thick incohesive unit of white to minty green massive fault gouge. In thin exposure, the gouge contains a brown clay-rich matrix with subangular to subrounded clasts of intensely fractured quartz up to 3 mm in size (Figure 6b). The relative proportions of matrix and clast by area are estimated to be 90% and 10% respectively (see Figure S2) This unit constitutes the fault core (sensu Caine et al., 1996), which was only found exposed at this location.

At Kalulu, the fault core is surrounded by a 5-15 m thick incohesive unit of quartzofeldspathic granulite and hornblende gneiss. At the other three other localities a 15-45 m wide unit of incohesive biotite ± hornblende ± pyroxene gneiss is found in the exposure closest to the scarp (Figure S3). Metamorphic foliation and pegmatite veins are still preserved within the incohesive gneisses; however, they may be locally separated by < 0.6 m along minor faults (Figure 6).

In the incohesive gneisses at Kanjedza, a 2 m wide ductile reverse shear zone has been exploited by a NW-SE striking dyke of unknown age (Figure 7). A minor fault with a normal sense of slip has then subsequently offset this dyke. At Mbewe, a 50 cm thick steeply dipping foliated fault gouge is present 10 m into the footwall and is parallel to the scarp. This gouge represents a fault that juxtaposes charnockite and hornblende gneisses (Figure S3). The hornblende gneiss foliation here is locally folded. At distances of more than 50-280 m from the fault at Kanjedza, Kalulu, and Muona, intact biotite ± hornblende gneisses are crosscut by vertical NE-SW striking dolerite dykes.

In thin sections made from the incohesive gneisses (i.e. within 45 m of the fault) at Kanjedza and Kalulu, quartz and feldspar grains exhibit fracture densities of 2.3-4.8 mm^{-1} (Figure 8). These fractures are oblique to the foliation, which is defined at the microscale by alternating quartzofeldspathic and biotite ± hornblende ± garnet bands, in which elongate biotite grains are aligned to and also define a foliation subparallel to the compositional banding. Fractures are generally intragranular and closed, with some rare cases of them hosting biotite or calcite mineralisation (Figure 8d). Open fractures are also observed and most prevalent in samples closest to the fault (Figure 8d). Microscale fracture density 50-280 m from the fault within the intact gneisses is 0.9-2.2 mm^{-1}, and fractures are parallel to the foliation (Figure 8f). We interpret the 15-45 m wide unit of incohesive gneiss with a relatively high fracture density, foliation-oblique fractures, and that has only accommodated a minor amount of displacement, as the footwall damage zone (sensu Caine et al., 1996) of the Thyolo fault.

No systematic decay in fracture density with distance from the fault is observed within the damage zone (Figure 8), which may reflect that samples are not consistently oriented with respect to the fault, and/or variations in grain size and composition. Alternatively, it may be due to the influence of minor faults within the damage zone; the highest fracture density is recorded ~42 m from the fault at Kanjedza, where a dyke has been offset by a minor fault, and abundant biotite veins are observed (Figure 8d). It is unclear whether this relatively high fracture density can be attributed to dyke emplacement or displacement on the minor fault The microfracture density increase inside the damage zone relative to the background level is relatively minor (Figure 8h*;* compare with (Wilson et al., 2003; Mitchell and Faulkner, 2009). However, it is difficult to assess if this is representative of a relatively low fracture density in the damage zone, or if it may reflect selective sampling of more cohesive, intact portions of the damage zone for thin section preparation and fracture density quantification.

5. Discussion

Topographic features including an 18.6 ± 7.7 m fault scarp and triangular facets indicate that the Thyolo fault has been reactivated during the current stage of East African Rifting. Whereas the Thyolo fault is dominantly subparallel to the metamorphic foliation, there are notable sections where the strike turns by 90˚ and therefore trends subparallel to Stormberg-age dolerite dykes (Figure 5). Here we discuss what defines fault segmentation where two different indicators of segmentation (geometrical changes and displacement profile minima) yield different numbers and locations of segment boundaries. We also discuss the fault zone structure in comparison to other rift-related faults, and how the reactivation of shallow crustal heterogeneities and deeper viscous deformation may combine to affect surface trace geometry. To conclude, we propose a model for the combined effects of pre-existing structures and dynamic stresses on fault reactivation.

5.1 Fault segmentation

Scarp height minima and changes in surface fault geometry are generally considered indicators of fault segment boundaries (Crone and Haller, 1991b; Machette et al., 1991; Peacock and Sanderson, 1991; Crider and Pollard, 1998; Mortimer et al., 2007, 2016; Fossen and Rotevatn, 2016). These factors identified matching segment numbers and boundary locations along the Bilila-Mtakataka fault in southern Malawi (Hodge et al., 2018b; see Figure 1 for location). However, along the Thyolo fault, the locations of scarp height minima do not coincide with changes in surface fault geometry (Figure 4). The sections that trend perpendicular to the overall strike range in length from 170 m to 4.8 km, but only one of the sections (the Chisumbi section) is likely long enough to be considered a geometrical segment boundary (i.e. ≥ ~3-5 km;

Wesnousky, 2008). This geometry has been used to argue that the Thyolo and Muona sections are different faults (Hodge et al., 2019). However, a fault scarp along the Chisumbi section links the Thyolo and Muona sections, and the height of this scarp is in the same range as scarps along the bounding Thyolo and Muona sections (Figure 3b, profile D; Figure 4b). This implies that during the recent events that formed the scarp, slip likely propagated along and through the 4.8 km long, ~100° bend in the fault. Given the ~600 m high escarpment and triangular facets along the Chisumbi section it is also likely that slip has propagated along and through this section over longer geological time (Figure 9c). This suggests that on faults that have reactivated pre-existing fabrics, purely geometrical criteria may not adequately identify fault segmentation for seismic hazard purposes. This is in contrast to the Wasatch fault zone, USA, where DuRoss et al. (2016) suggest that displacement profiles have limited value for identifying segment boundaries that restrict earthquake ruptures.

The Chisumbi section lacks evidence for distributed strain in the area between the tips of the Thyolo and Muona sections it links (Figure 9). There is no or minor anticlockwise rotation of dykes in the footwall of the Chisumbi section and the slope dips at a very shallow angle (~2°). This suggests that little strain accumulated within this section prior to the bounding Thyolo and Muona sections becoming linked (Willemse et al., 1996; Peacock and Sanderson, 1991; Densmore et al., 2003; Fossen and Rotevatn, 2016; Figure 9). Through this lack of evidence for the development of a relay ramp, we therefore propose that the Thyolo and Muona sections are linked by weak structures that have been activated in the shallow upper crust, but which do not operate as permanent barriers to earthquake rupture and propagation (Figure 9d). The Chisumbi linkage zone also differs in geomorphology from a typical relay ramp (e.g. Gawthorpe and Leeder, 2000; Densmore et al., 2003), with no axial ramp drainage, but also no transverse ramp drainage (Figures 5 and 9). Instead the main drainage channel runs along the overlapping tip of the Thyolo section leading to an abnormal configuration to the hanging wall alluvial fans (Figures 5 and 9). This suggests that where pre-existing structures affect the reactivation of extensional basins, unusual patterns of sediment transport and deposition may be observed.

5.2 Thyolo fault zone structure

Normal faults grow incrementally by a combination of accumulation of displacement, linkage of segments, and increase in length, such that fault growth, structure, and geometry are closely linked (e.g. Cartwright et al., 1996; Childs et al., 2017; Hodge et al., 2018a; Rotevatn et al., 2019). Along the Thyolo fault, we cannot place definitive constraints on the total damage zone width or displacement, because we lack hanging wall exposures and distinct marker horizons. Nevertheless, given its ~1 km (Figure 1c) escarpment height and a fault dip of ~ 60° (Williams et al., 2019), it must have accommodated >1.2 km of net dip-slip displacement. Furthermore, although damage zones are typically asymmetric, the hanging wall damage zone rarely exceeds three times the width of the footwall damage zone where both are exposed (Beach et al., 1999; Shipton and Cowie, 2001; Berg and Skar, 2005; Kristensen et al., 2016), and in some cases, the damage zone may be wider in the footwall than the hanging wall (Biegel and Sammis, 2004). With a footwall damage zone 15-45 m wide, we therefore suggest that the entire width of the Thyolo fault damage zone is between 15 and 180 m.

Given a displacement of 1.2 km, the Thyolo fault damage zone width is within the range of displacement vs damage zone width determined from compilations of all fault types (Torabi and Berg, 2011; Savage and Brodsky, 2011). However, there is considerable scatter in these plots owing to variations in the fault kinematics, lithology, and the depth of faulting. A more instructive comparison may therefore be to the Djomberg fault in Greenland, which offers a rare example of a well exposed rift border fault (3 km throw) in crystalline metamorphic basement rocks (Kristensen et al., 2016). The Djomberg fault's damage zone extends 600 m into the footwall (Kristensen et al., 2016), which is 10 times further than the Thyolo fault, although both faults are parallel to a gneissic footwall foliation.

Fault core thickness also scales with displacement, with the km-scale slip along the Thyolo fault predicted to result in a fault core 1-10 m thick (Torabi and Berg, 2011; Torabi et al., 2019). Across the Djomberg fault slip is accommodated across several <50 cm thick strands of gouge and breccia in a 200 m wide zone within the fault's footwall (Kristensen et al., 2016). However, along the Thyolo fault, the fault core is 0.7 m thick at Kalulu (Figure 6), and although the fault core is not exposed elsewhere, the footwall damage zone extends to within 15 m of the scarp at Kanjedza placing a maximum constraint on footwall fault core thickness at 15 m here. At Mbewe (see Figure 3 for location), the damage zone extends to within 1 m of the scarp; however, there is a secondary fault strand 10 m into the footwall. In summary, the damage zone width of the Thyolo fault is therefore comparable to other faults with km scale displacement; however, it is relatively narrow compared to another example of a rift border fault, and its slip is localised into an anomalously narrow fault core given the displacement it has accommodated.

5.3 Mechanism of fault reactivation

Within amagmatic portions of the East African Rift System, immature faults (Biggs et al., 2010), strong, cold intact crust (Fagereng, 2013) and low b-values recorded during seismic sequences (Gaherty et al., 2019; Lavayssière et al., 2019) are all suggestive of high differential stress in the region. Furthermore, gouge sampled from the fault core at Kalulu does not contain significant amounts of frictionally weak minerals (Williams et al., 2019), and deformation experiments on representative lithologies from the Malawi Rift indicate that they are frictionally strong (coefficient of friction, μ_s >0.55; Hellebrekers et al., 2019). However, the fault is generally oriented parallel or sub-parallel to basement foliation and possibly also Karoo-age dykes (Figure 4-5). These structures may provide low cohesion planes for frictional reactivation, even if they are slightly oblique to the minimum principal compressive stress (Williams et al., 2019).

Previous studies indicate that complex surface patterns of normal faults may connect to a more planar feature at depth (e.g. Graymer et al., 2007; Walker et al., 2017; Hodge et al., 2018). We suggest that interlinked mechanisms of reactivation and dynamic stress reorientation along the Thyolo fault may explain the geometry of fault sections orientated perpendicular to the strike of the main fault and sub-parallel to Stormberg dykes. Firstly, the overlapping geometry between the Thyolo and Muona sections may have been established early in the growth history of the Thyolo fault. This overlapping geometry favours high angle link structures formed due to coseismic Coulomb stress changes on the bounding faults (Hodge et al., 2018a)., rather than obliquely oriented breached relay ramps or the creation of a fault bend. These links may have originated as transform faults, and later seen reactivation as normal faults, although no evidence for transform motion is preserved. Secondly, slip on orthogonal structures may have been favoured by the presence of dolerite dykes perpendicular to the Thyolo fault (Figure 5a), although linking segments coinciding with a pre-existing dyke have not been directly observed. Dolerite dykes emplaced within Karoo sediments in South Africa have been reported to induce increased brittle damage reducing cohesion along the dyke-basement contact zone (Senger et al., 2015). It is therefore possible that co-seismic stress changes on overlapping faults favoured shallow activation of low-cohesion zones at the edge of the pre-existing dykes.

We suggest that low cohesion planes may play an important role in controlling fault geometry in the shallow crust. Though significant fluid flow can result in fault zone cohesion regaining its strength relatively quickly (10^3-10^5 years; Tenthorey and Cox 2006), this recovery mechanism is unlikely along the Thyolo fault as the crust in Malawi has been dehydrated during one or more previous episodes of high grade metamorphism (Fagereng, 2013). Furthermore, we do not see fault zone fluid flow indicators in our microstructural and field observations (e.g. no extensive vein networks or fault zone alteration; Wästeby et al., 2014; Williams et al., 2017) and instead find evidence for an incohesive ‘unhealed’ fault damage zone (Figures 7 & 8).

While the fault may follow near-surface weaknesses, this mechanism is less applicable at depths where cohesion is maintained or confining stresses too high for frictional failure. The Thyolo fault is located at or towards the edge of the Unango Terrane, although the exact nature and location of this boundary is uncertain. If it is similar to other high metamorphic grade boundaries, it could represent an existing shear zone that is viscously weak because of small grain size (Watterson, 1975; Fliervoet et al., 1997; Stenvall et al., 2019), foliation of interconnected low viscosity minerals (Handy, 1990; Montési, 2013), crystal-preferred orientations conducive to plastic flow (Poirier, 1980), or provide a competency contrast across the boundary that leads to increased stress and therefore a localisation of strain (Goodwin and Tikoff, 2002). Thus, we suggest that heterogeneity in viscous processes associated with ductile structures can localise strain beneath the brittle crust along the Thyolo fault. Consequently, we consider that the Thyolo fault follows a deep-seated ductile weakness associated with the boundary of the Unango Terrane at mid-crustal level and exploits low cohesion, well oriented foliation planes linked by dyke edges at the near surface (Figure 10).

A deep-seated ductile control on the overall fault structure and displacement may explain why along the Thyolo fault, shallow structures have induced changes in fault geometry that are not reflected in the scarp height. Hence, although many faults, including the Bilila-Mtakataka fault in the Makanjira Graben (Figure 1; Hodge et al., 2018b), show both displacement minima and geometrical changes (or structural complexity) at the same locations (Peacock and Sanderson, 1991; Dawers and Anders, 1995; Walsh et al., 2003), where a fault experiences depth-dependent control on its structures, these two segmentation criteria are unlikely to agree. This presents a challenge when segmentation criteria based on shallow structures is used for assessing earthquake magnitudes for seismic hazard analyses (e.g. Field et al., 2009; Petersen et al., 2015; Valentini et al., 2019): where depth-dependent segmentation is not correctly identified, multi-segment and multi-fault ruptures such as those observed in the 2016 earthquakes in central Italy (M_w6.2, 6.1 & 6.6) and Kaikoura, New Zealand (M_w7.8) or the 2010 M_w7.2 El Mayor-Cucapah, Mexico earthquake (Wei et al., 2011; Hamling et al., 2017; Walters et al., 2018) may become more likely than is apparent from superficial indicators of fault segmentation.

A depth-dependent combination of structural controls can also explain other observations along the Thyolo fault, including its slightly oblique orientation to the regional extension direction yet apparent dip-slip kinematics (Philippon et al., 2015; Hodge et al., 2018b; Williams et al., 2019) and its continual reactivation under a diverse range of previous extensional directions within the Lower Shire Graben (Castaing, 1991). Furthermore, localised slip and a narrow damage zone is also observed for other faults that follow a pre-existing foliation (Heermance et al., 2003; Zangerl et al., 2006). Thus, through collective evidence for structural controls and fast fault growth in a localised fault core, we prefer an interpretation where fault geometry is controlled by heterogeneities in the viscous lower crust, with the brittle upper crust having a secondary control affecting the surface trace. We recognise the model where the primary control on rift growth is lithospheric strength (Ebinger et al., 1991); however, while the total fault length may indeed reflect a thick elastic crust, the detailed fault geometry appears affected by documented structural elements.

5.4 Comparison with other continental rifts and grabens

That shallow brittle structures only have a superficial, geometric effect on fault segmentation is important, because geometrical criteria have been used to define fault segments for seismic hazard purposes (Crone and Haller, 1991a; Lettis et al., 2002; Wesnousky, 2008). If local fabrics only control the shallow orientation of the fault, this also explains why faults in Malawi have been simultaneously observed to crosscut and follow the metamorphic foliation (Hodge et al., 2018b). Furthermore, it explains the difference between the Lower Shire Graben, where the largest topographic relief indicates that the majority of displacement occurs on the border fault (the Thyolo fault; Fig. 1), and the Zomba Graben to the north, where displacement is distributed more evenly between border and intrabasin faults (Wedmore et al., 2019). Lateral heterogeneity within the lower crust beneath the Zomba Graben has been inferred to cause this more heterogeneous strain distribution, possibly by multiple localised shear zones at depth guiding distributed deformation in the upper crust and at the surface (Wedmore et al., 2019). This is a preferred explanation for strain distribution in the Zomba Graben, as it is located *within* the Unango Terrane. In contrast, the Lower Shire Graben is located towards the edge of the terrane boundary and hence the deformation may localise towards the terrane edge. This localised deformation and fast growth and linkage of a border fault is comparable to the Okavango rift, which is also inferred to be localised along a long-lived pre-existing crustal-scale weak zone (Kinabo et al., 2007, 2008).

The northern North Sea basin is another example of a multiphase rift where faults are hosted in crystalline basement rocks. Here, lithospheric thinning and heating, as well as stress feedbacks between growing faults, control the rift-scale localisation of strain, with pre-existing shallow brittle faults thought to have little control on reactivation (Cowie et al., 2005; Claringbould et al., 2017). Our results are consistent with the inference that pre-existing shallow structures and fabrics have only minor control on reactivation, and that pre-existing upper crustal faults play only a minor, superficial role in controlling subsequent rift geometries in crystalline, dry, continental crust. This differs from studies where a major role in rift evolution has been suggested for upper crustal faults (e.g. Bellahsen & Daniel, 2005; Duffy et al., 2015; Heilman et al., 2019; Katumwehe et al., 2015; Laõ-Dávila et al., 2015; Whipp et al., 2014). This confirms the need to consider the scale and depth dependence of the influence of pre-existing structures when assessing fault reactivation, where the pre-existing weaknesses may control macro- but not meso-scale structural development (Kirkpatrick et al., 2013; Samsu et al., 2020).

6. Conclusion

The Thyolo fault is the major border fault within the Lower Shire Graben, which has experienced Neoproterozoic continental collision and at least three previous periods of Phanerozoic rifting. Using high resolution topography, we mapped the surface trace of the Thyolo fault to study the reactivation of the fault within the current period of rifting in East Africa. Long sections of the fault have a NW-SE strike, but these are separated by short sections that strike NE-SW. The largest NE-SW section is 4.8 km long, which is normally considered long enough to define a separate fault segment that accumulates displacement differently from adjacent segments. However, based on along strike variations of the height of the active fault scarp, we find three main segments, each with a scarp approximately 20 m high. The segment boundaries defined by the scarp height do not correspond to prominent geometrical changes in fault strike that are normally considered indicative of segment boundaries. We find that the fault and pre-existing foliation are broadly parallel, whereas the strike of the short sections orientated NE-SW matches the strike of dykes emplaced during a previous period of rifting in the Karoo. Using field and microstructural observations of the Thyolo fault's footwall, we estimate that the entire fault zone is between 15-180 m wide, comparable to other faults of similar displacement, but considerably narrower than another example of a rift bounding fault in crystalline metamorphic basement (the Djomberg fault, Greenland). All these observations suggest that the shallow portion of the fault is reactivating well-oriented foliation planes and perpendicularly oriented dyke contacts that act as low-cohesion surfaces in the shallow crust. However, these pre-existing structures are not reflected in the displacement-length profile, and are therefore interpreted as not being able to affect the growth and segmentation of the reactivated fault. Instead, we suggest that the fundamental control on the growth and displacement accumulation of this rift border fault is controlled by reactivation in the viscous regime, of mid-crustal ductile heterogeneities associated with the edge of the Unango Terrane.

7. Acknowledgements

This work was funded by the EPSRC project 'Prepare' (EP/P028233/1), funded under the Global Challenges Research Fund. We thank Kondwani Dombola for his assistance with fieldwork planning and logistics. TanDEM-X data were obtained via DLR proposal DEM_GEOL0686.

References

Beach, A., Welbon, A.I., Brockbank, P.J., and McCallum, J.E., 1999, Reservoir damage around faults: Outcrop examples from the Suez rift: Petroleum Geoscience, v. 5, p. 109–116, doi:10.1144/petgeo.5.2.109.

Bellahsen, N., and Daniel, J.M., 2005, Fault reactivation control on normal fault growth: An experimental study: Journal of Structural Geology, v. 27, p. 769–780, doi:10.1016/j.jsg.2004.12.003.

Berg, S.S., and Skar, T., 2005, Controls on damage zone asymmetry of a normal fault zone: Outcrop analyses of a segment of the Moab fault, SE Utah: Journal of Structural Geology, v. 27, p. 1803–1822, doi:10.1016/j.jsg.2005.04.012.

Biegel, R.L., and Sammis, C.G., 2004, Relating Fault Mechanics to Fault Zone Structure, *in* Advances in Geophysics, p. 65–111, doi:10.1016/S0065-2687(04)47002-2.

Biggs, J., Nissen, E., Craig, T., Jackson, J., and Robinson, D.P., 2010, Breaking up the hanging wall of a rift-border fault: The 2009 Karonga earthquakes, Malawi: Geophysical Research Letters, v. 37, p. 1–5, doi:10.1029/2010GL043179.

Bingen, B., Jacobs, J., Viola, G., Henderson, I.H.C., Skår, Ø., Boyd, R., Thomas, R.J., Solli, A., Key, R.M., and Daudi, E.X.F., 2009, Geochronology of the Precambrian crust in the Mozambique belt in NE Mozambique, and implications for Gondwana assembly: Precambrian Research, v. 170, p. 231–255, doi:10.1016/j.precamres.2009.01.005.

Bloomfield, K., 1965, The geology of the Zomba Area: Bulletin of the Geological Survey, Malawi, v. 16.

Buck, W.R., 1991, Modes of continental lithospheric extension: Journal of Geophysical Research: Solid Earth, v. 96, p. 20161–20178, doi:10.1029/91JB01485.

Caine, J.S., Evans, J.P., and Forster, C.B., 1996, Fault zone architecture and permeability structure: Geology, v. 24, p. 1025–1028, doi:10.1130/0091-7613(1996)024<1025:FZAAPS>2.3.CO;2.

Cartwright, J.A., Mansfield, C., and Trudgill, B., 1996, The growth of normal faults by segment linkage: Geological Society, London, Special Publications, v. 99, p. 163–177, doi:10.1144/GSL.SP.1996.099.01.13.

Castaing, C., 1991, Post-Pan-African tectonic evolution of South Malawi in relation to the Karroo and recent East African rift systems: Tectonophysics, v. 191, p. 55–73, doi:10.1016/0040-1951(91)90232-H.

Childs, C., Holdsworth, R.E., Jackson, C.A.L., Manzocchi, T., Walsh, J.J., and Yielding, G., 2017, Introduction to the geometry and growth of normal faults: Geological Society Special Publication, v. 439, p. 1–9, doi:10.1144/SP439.24.

Childs, C., Manzocchi, T., Walsh, J.J., Bonson, C.G., Nicol, A., and Schöpfer, M.P.J., 2009, A geometric model of fault zone and fault rock thickness variations: Journal of Structural Geology, v. 31, p. 117–127, doi:10.1016/j.jsg.2008.08.009.

Chisenga, C., Dulanya, Z., and Jianguo, Y., 2019, The structural re-interpretation of the Lower Shire Basin in the Southern Malawi rift using gravity data: Journal of African Earth Sciences, v. 149, p. 280–290, doi:10.1016/j.jafrearsci.2018.08.013.

Chorowicz, J., 2005, The East African rift system: Journal of African Earth Sciences, v. 43, p. 379–410, doi:10.1016/j.jafrearsci.2005.07.019.

Chorowicz, J., and Sorlien, C., 1992, Oblique extensional tectonics in the Malawi Rift, Africa: Geological Society of America Bulletin, v. 104, p. 1015–1023, doi:10.1130/0016-7606(1992)104<1015:OETITM>2.3.CO;2.

Claringbould, J.S., Bell, R.E., Jackson, C.A.L., Gawthorpe, R.L., and Odinsen, T., 2017, Pre-existing normal faults have limited control on the rift geometry of the northern North Sea: Earth and Planetary Science Letters, v. 475, p. 190–206, doi:10.1016/j.epsl.2017.07.014.

Collettini, C., and Sibson, R.H., 2001, Normal faults, normal friction? Geology, v. 29, p. 927, doi:10.1130/0091-7613(2001)029<0927:NFNF>2.0.CO;2.

Cowie, P.A., 1998, A healing-reloading feedback control on the growth rate of seismogenic faults: Journal of Structural Geology, v. 20, p. 1075–1087, doi:10.1016/S0191-8141(98)00034-0.

Cowie, P.A., and Scholz, C.H., 1992a, Displacement-length scaling relationship for faults: data synthesis and discussion: Journal of Structural Geology, v. 14, p. 1149–1156, doi:10.1016/0191-8141(92)90066-6.

Cowie, P.A., and Scholz, C.H., 1992b, Growth of faults by accumulation of seismic slip: Journal of Geophysical Research, v. 97, p. 11085, doi:10.1029/92JB00586.

Cowie, P.A., and Scholz, C.H., 1992c, Physical explanation for the displacement-length relationship of faults using a post-yield fracture mechanics model: Journal of Structural Geology, v. 14, p. 1133–1148, doi:10.1016/0191-8141(92)90065-5.

Cowie, P.A., Underhill, J.R., Behn, M.D., Lin, J., and Gill, C.E., 2005, Spatio-temporal evolution of strain accumulation derived from multi-scale observations of Late Jurassic rifting in the northern North Sea: A critical test of models for lithospheric extension: Earth and Planetary Science Letters, v. 234, p. 401–419, doi:10.1016/j.epsl.2005.01.039.

Craig, T.J., Jackson, J.A., Priestley, K., and Mckenzie, D., 2011, Earthquake distribution patterns in Africa: Their relationship to variations in lithospheric and geological structure, and their rheological implications: Geophysical Journal

International, v. 185, p. 403–434, doi:10.1111/j.1365-246X.2011.04950.x.

Crider, J.G., and Pollard, D.D., 1998, Fault linkage: Three-dimensional mechanical interaction between echelon normal faults: Journal of Geophysical Research: Solid Earth, v. 103, p. 24373–24391, doi:10.1029/98jb01353.

Crone, A.J., and Haller, K.M., 1991a, Segmentation and the coseismic behavior of Basin and Range normal faults: examples from east-central Idaho and southwestern Montana, U.S.A.: Journal of Structural Geology, v. 13, p. 151–164, doi:10.1016/0191-8141(91)90063-O.

Crone, A.J., and Haller, K.M., 1991b, Segmentation and the coseismic behavior of Basin and Range normal faults: examples from east-central Idaho and southwestern Montana, U.S.A.: Journal of Structural Geology, v. 13, p. 151–164, doi:10.1016/0191-8141(91)90063-O.

Daly, M.C., Chorowicz, J., and Fairhead, J.D., 1989, Rift basin evolution in Africa: The influence of reactivated steep basement shear zones: Geological Society Special Publication, v. 44, p. 309–334, doi:10.1144/GSL.SP.1989.044.01.17.

Dawers, N.H., and Anders, M.H., 1995, Displacement-length scaling and fault linkage: Journal of Structural Geology, v. 17, p. 607–614, doi:10.1016/0191-8141(94)00091-D.

Dawers, N.H., Anders, M.H., and Scholz, C.H., 1993, Growth of normal faults: displacement-length scaling: Geology, v. 21, p. 1107–1110, doi:10.1130/0091-7613(1993)021<1107:GONFDL>2.3.CO;2.

Densmore, A.L., Dawers, N.H., Gupta, S., Allen, P.A., and Gilpin, R., 2003, Landscape evolution at extensional relay zones: Journal of Geophysical Research: Solid Earth, v. 108, p. 1–15, doi:10.1029/2001jb001741.

Dixey, F., and Campbell Smith, W., 1929, The rocks of the Lupata Gorge and the north side of the lower Zambezi: Geological Magazine, v. 66, p. 241–259.

Duffy, O.B., Bell, R.E., Jackson, C.A.L., Gawthorpe, R.L., and Whipp, P.S., 2015, Fault growth and interactions in a multiphase rift fault network: Horda Platform, Norwegian North Sea: Journal of Structural Geology, v. 80, p. 99–119, doi:10.1016/j.jsg.2015.08.015.

DuRoss, C.B., Personius, S.F., Crone, A.J., Olig, S.S., Hylland, M.D., Lund, W.R., and Schwartz, D.P., 2016, Fault segmentation: New concepts from the Wasatch Fault Zone, Utah, USA: Journal of Geophysical Research: Solid Earth, v. 121, p. 1131–1157, doi:10.1002/2015JB012519.

Ebinger, C., 2005, Continental break-up: The East African perspective: Astronomy and Geophysics, v. 46, p. 2.16-2.21, doi:10.1111/j.1468-4004.2005.46216.x.

Ebinger, C.J., 1989, Geometric and kinematic development of border faults and accommodation zones, Kivu-Rusizi Rift, Africa: Tectonics, v. 8, p. 117–133, doi:10.1029/TC008i001p00117.

Ebinger, C., Djomani, Y.P., Mbede, E., Foster, A., and Dawson, J.B., 1997, Rifting Archaean lithosphere: the Eyasi-Manyara-Natron rifts, East Africa: Journal of the Geological Society, v. 154, p. 947–960, doi:10.1144/gsjgs.154.6.0947.

Ebinger, C.J., Karner, G.D., and Weissel, J.K., 1991, Mechanical strength of extended continental lithosphere: Constraints from the Western Rift System, East Africa: Tectonics, v. 10, p. 1239–1256, doi:10.1029/91TC00579.

Eby, G.N., Roden-Tice, M., Krueger, H.L., Ewing, W., Faxon, E.H., and Woolley, A.R., 1995, Geochronology and cooling history of the northern part of the Chilwa Alkaline Province, Malawi: Journal of African Earth Sciences, v. 20, p. 275–288, doi:10.1016/0899-5362(95)00054-W.

Fagereng, Å., 2013, Fault segmentation, deep rift earthquakes and crustal rheology:

Insights from the 2009 Karonga sequence and seismicity in the Rukwa-Malawi rift zone: Tectonophysics, v. 601, p. 216–225, doi:10.1016/j.tecto.2013.05.012.

Field, E.H. et al., 2009, Uniform California Earthquake Rupture Forecast, Version 2 (UCERF 2): Bulletin of the Seismological Society of America, v. 99, p. 2053–2107, doi:10.1785/0120080049.

Fliervoet, T.F., White, S.H., and Drury, M.R., 1997, Evidence for dominant grain-boundary sliding deformation in greenschist- and amphibolite-grade polymineralic ultramylonites from the Redbank Deformed Zone, Central Australia: Journal of Structural Geology, v. 19, p. 1495–1520, doi:10.1016/S0191-8141(97)00076-X.

Fossen, H., and Rotevatn, A., 2016, Fault linkage and relay structures in extensional settings-A review: Earth-Science Reviews, v. 154, p. 14–28, doi:10.1016/j.earscirev.2015.11.014.

Fullgraf, T., Dombola, K., Hyvonen, E., Thomas, B., and Zammit, C. The Provisional GEMMAP 1:1 Million Scale structural and geological maps of Malawi: Geological Survey of Malawi,.

Gaherty, J.B. et al., 2019, Faulting processes during early-stage rifting: Seismic and geodetic analysis of the 2009-2010 Northern Malawi earthquake sequence: Geophysical Journal International, v. 217, p. 1767–1782, doi:10.1093/gji/ggz119.

Gawthorpe, R.L., Jackson, C.A.-L., Young, M.J., Sharp, I.R., Moustafa, A.R., and Leppard, C.W., 2003, Normal fault growth, displacement localisation and the evolution of normal fault populations: the Hammam Faraun fault block, Suez rift, Egypt: Journal of Structural Geology, v. 25, p. 883–895, doi:10.1016/S0191-8141(02)00088-3.

Gawthorpe, R.L., and Leeder, M.R., 2000, Tectono-sedimentary evolution of active extensional basins: Basin Research, v. 12, p. 195–218, doi:10.1111/j.1365-2117.2000.00121.x.

Giba, M., Walsh, J.J., and Nicol, A., 2012, Segmentation and growth of an obliquely reactivated normal fault: Journal of Structural Geology, v. 39, p. 253–267, doi:10.1016/j.jsg.2012.01.004.

Goodwin, L.B., and Tikoff, B., 2002, Competency contrast, kinematics, and the development of foliations and lineations in the crust: Journal of Structural Geology, v. 24, p. 1065–1085, doi:10.1016/S0191-8141(01)00092-X.

Graymer, R.W., Langenheim, V.E., Simpson, R.W., Jachens, R.C., and Ponce, D.A., 2007, Relatively simple through-going fault planes at large-earthquake depth may be concealed by the surface complexity of strike-slip faults: Geological Society, London, Special Publications, v. 290, p. 189–201, doi:10.1144/SP290.5.

Gupta, A., and Scholz, C.H., 2000, A model of normal fault interaction based on observations and theory: Journal of Structural Geology, v. 22, p. 865–879, doi:10.1016/S0191-8141(00)00011-0.

Habgood, F., 1963, The geology of the country west of the Shire River between Chikwawa and Chiromo: Bulletin of the Geological Survey, Malawi, v. 14.

Habgood, F., Holt, D.N., and Walshaw, R.D., 1973, The geology of the Thyolo Area: Bulletin of the Geological Survey, Malawi, v. 22.

Hamling, I.J. et al., 2017, Complex multifault rupture during the 2016 Mw 7.8 Kaikōura earthquake, New Zealand: Science, v. 356, doi:10.1126/science.aam7194.

Handy, M.R., 1990, The solid-state flow of polymineralic rocks: Journal of

Geophysical Research, v. 95, p. 8647, doi:10.1029/JB095iB06p08647.

Healy, D., Rizzo, R.E., Cornwell, D.G., Farrell, N.J.C., Watkins, H., Timms, N.E., Gomez-Rivas, E., and Smith, M., 2017, FracPaQ: A MATLABTM toolbox for the quantification of fracture patterns: Journal of Structural Geology, v. 95, p. 1–16, doi:10.1016/j.jsg.2016.12.003.

Heermance, R., Shipton, Z.K., and Evans, J.P., 2003, Fault structure control on fault slip and ground motion during the 1999 rupture of the Chelungpu fault, Taiwan: Bulletin of the Seismological Society of America, v. 93, p. 1034–1050, doi:10.1785/0120010230.

Heilman, E., Kolawole, F., Atekwana, E.A., and Mayle, M., 2019, Controls of Basement Fabric on the Linkage of Rift Segments: Tectonics, v. 38, p. 1337–1366, doi:10.1029/2018TC005362.

Hellebrekers, N., Niemeijer, A.R., Fagereng, Å., Manda, B., and Mvula, R.L.S., 2019, Lower crustal earthquakes in the East African Rift System: Insights from frictional properties of rock samples from the Malawi rift: Tectonophysics, v. 767, p. 228167, doi:10.1016/j.tecto.2019.228167.

Henstra, G.A., Rotevatn, A., Gawthorpe, R.L., and Ravnås, R., 2015, Evolution of a major segmented normal fault during multiphase rifting: The origin of plan-view zigzag geometry: Journal of Structural Geology, v. 74, p. 45–63, doi:10.1016/j.jsg.2015.02.005.

Henza, A.A., Withjack, M.O., and Schlische, R.W., 2011, How do the properties of a pre-existing normal-fault population influence fault development during a subsequent phase of extension? Journal of Structural Geology, v. 33, p. 1312–1324, doi:10.1016/j.jsg.2011.06.010.

Hodge, M., Biggs, J., Fagereng, Å., Elliott, A., Mdala, H., and Mphepo, F., 2019, A semi-automated algorithm to quantify scarp morphology (SPARTA): Application to normal faults in southern Malawi: Solid Earth, v. 10, p. 27–57, doi:10.5194/se-10-27-2019.

Hodge, M., Fagereng, and Biggs, J., 2018a, The Role of Coseismic Coulomb Stress Changes in Shaping the Hard Link Between Normal Fault Segments: Journal of Geophysical Research: Solid Earth, v. 123, p. 797–814, doi:10.1002/2017JB014927.

Hodge, M., Fagereng, Biggs, J., and Mdala, H., 2018b, Controls on Early-Rift Geometry: New Perspectives From the Bilila-Mtakataka Fault, Malawi: Geophysical Research Letters, v. 45, p. 3896–3905, doi:10.1029/2018GL077343.

Holdsworth, R.E., Butler, C.A., and Roberts, A.M., 1997, The recognition of reactivation during continental deformation: Journal of the Geological Society, v. 154, p. 73–78, doi:10.1144/gsjgs.154.1.0073.

Hollinsworth, A.D., Koehn, D., Dempster, T.J., and Aanyu, K., 2019, Structural controls on the interaction between basin fluids and a rift flank fault: Constraints from the Bwamba Fault, East African Rift: Journal of Structural Geology, v. 118, p. 236–249, doi:10.1016/j.jsg.2018.10.012.

Johnson, K., Nissen, E., Saripalli, S., Arrowsmith, J.R., McGarey, P., Scharer, K., Williams, P., and Blisniuk, K., 2014, Rapid mapping of ultrafine fault zone topography with structure from motion: Geosphere, v. 10, p. 969–986, doi:10.1130/GES01017.1.

Johnson, S.P., Rivers, T., and De Waele, B., 2005, A review of the Mesoproterozoic to early Palaeozoic magmatic and tectonothermal history of south–central Africa: implications for Rodinia and Gondwana: Journal of the Geological

Society, v. 162, p. 433–450, doi:10.1144/0016-764904-028.

Karmakar, S., and Schenk, V., 2016, Mesoproterozoic UHT metamorphism in the Southern Irumide Belt, Chipata, Zambia: Petrology and in situ monazite dating: Precambrian Research, v. 275, p. 332–356, doi:10.1016/j.precamres.2016.01.018.

Katumwehe, A.B., Abdelsalam, M.G., and Atekwana, E.A., 2015, The role of pre-existing Precambrian structures in rift evolution: The Albertine and Rhino grabens, Uganda: Tectonophysics, v. 646, p. 117–129, doi:10.1016/j.tecto.2015.01.022.

Kinabo, B.D., Atekwana, E.A., Hogan, J.P., Modisi, M.P., Wheaton, D.D., and Kampunzu, A.B., 2007, Early structural development of the Okavango rift zone, NW Botswana: Journal of African Earth Sciences, v. 48, p. 125–136, doi:10.1016/j.jafrearsci.2007.02.005.

Kinabo, B.D., Hogan, J.P., Atekwana, E.A., Abdelsalam, M.G., and Modisi, M.P., 2008, Fault growth and propagation during incipient continental rifting: Insight from a combined aeromagnetic and Shuttle Radar Topography Mission digital elevation model investigation of the Okavango Rift Zone, northwest Botswana: Tectonics, v. 27, p. 1–16, doi:10.1029/2007TC002154.

Kirkpatrick, J.D., Bezerra, F.H.R., Shipton, Z.K., Do Nascimento, A.F., Pytharouli, S.I., Lunn, R.J., and Soden, A.M., 2013, Scale-dependent influence of pre-existing basement shear zones on rift faulting: A case study from NE Brazil: Journal of the Geological Society, v. 170, p. 237–247, doi:10.1144/jgs2012-043.

Kristensen, T.B., Rotevatn, A., Peacock, D.C.P., Henstra, G.A., Midtkandal, I., and Grundvåg, S.A., 2016, Structure and flow properties of syn-rift border faults: The interplay between fault damage and fault-related chemical alteration (Dombjerg

Fault, Wollaston Forland, NE Greenland): Journal of Structural Geology, v. 92, p. 99–115, doi:10.1016/j.jsg.2016.09.012.

Kröner, A., Willner, A.P., Hegner, E., Jaeckel, P., and Nemchin, A., 2001, Single zircon ages, PT evolution and Nd isotopic systematics of high-grade gneisses in southern Malawi and their bearing on the evolution of the Mozambique belt in southeastern Africa: Precambrian Research, v. 109, p. 257–291, doi:10.1016/S0301-9268(01)00150-4.

Laõ-Dávila, D.A., Al-Salmi, H.S., Abdelsalam, M.G., and Atekwana, E.A., 2015, Hierarchical segmentation of the Malawi Rift: The influence of inherited lithospheric heterogeneity and kinematics in the evolution of continental rifts: Tectonics, v. 34, p. 2399–2417, doi:10.1002/2015TC003953.

Lavayssière, A., Drooff, C., Ebinger, C., Gallacher, R., Illsley-Kemp, F., Oliva, S.J., and Keir, D., 2019, Depth Extent and Kinematics of Faulting in the Southern Tanganyika Rift, Africa: Tectonics, v. 38, p. 842–862, doi:10.1029/2018TC005379.

Leeder, M.R., and Gawthorpe, R.L., 1987, Sedimentary models for extensional tilt-block/half-graben basins: Geological Society, London, Special Publications, v. 28, p. 139–152, doi:10.1144/GSL.SP.1987.028.01.11.

Lettis, W., Bachhuber, J., Witter, R., Brankman, C., Randolph, C.E., Barka, A., Page, W.D., and Kaya, A., 2002, Influence of Releasing Step-Overs on Surface Fault Rupture and Fault Segmentation: Examples from the 17 August 1999 Izmit Earthquake on the North Anatolian Fault, Turkey: Bulletin of the Seismological Society of America, v. 92, p. 19–42, doi:10.1785/0120000808.

Macdonald, R., Crossley, R., and Waterhouse, K.S., 1983, Karroo basalts of southern Malawi and their regional petrogenetic significance: Mineralogical

Magazine, v. 47, p. 281–289, doi:10.1180/minmag.1983.047.344.02.

Macey, P.H. et al., 2010, Mesoproterozoic geology of the Nampula Block, northern Mozambique: Tracing fragments of Mesoproterozoic crust in the heart of Gondwana: Precambrian Research, v. 182, p. 124–148, doi:10.1016/j.precamres.2010.07.005.

Machette, M.N., Personius, S.F., Nelson, A.R., Schwartz, D.P., and Lund, W.R., 1991, The Wasatch fault zone, utah—segmentation and history of Holocene earthquakes: Journal of Structural Geology, v. 13, p. 137–149, doi:10.1016/0191-8141(91)90062-N.

Manda, B.W.C., Cawood, P.A., Spencer, C.J., Prave, T., Robinson, R., and Roberts, N.M.W., 2019, Evolution of the Mozambique Belt in Malawi constrained by granitoid U-Pb, Sm-Nd and Lu-Hf isotopic data: Gondwana Research, v. 68, p. 93–107, doi:10.1016/j.gr.2018.11.004.

McConnell, R.B., 1967, The East African Rift System: Nature, v. 215, p. 578–581, doi:10.1038/215578a0.

Mitchell, T.M., and Faulkner, D.R., 2009, The nature and origin of off-fault damage surrounding strike-slip fault zones with a wide range of displacements: A field study from the Atacama fault system, northern Chile: Journal of Structural Geology, v. 31, p. 802–816, doi:10.1016/j.jsg.2009.05.002.

Montési, L.G.J., 2013, Fabric development as the key for forming ductile shear zones and enabling plate tectonics: Journal of Structural Geology, v. 50, p. 254–266, doi:10.1016/j.jsg.2012.12.011.

Morewood, N.C., and Roberts, G.P., 2000, The geometry, kinematics and rates of deformation within an en echelon normal fault segment boundary, central Italy: Journal of Structural Geology, v. 22, p. 1027–1047, doi:10.1016/S0191-

8141(00)00030-4.

Morley, C.K., 2010, Stress re-orientation along zones of weak fabrics in rifts: An explanation for pure extension in ‘oblique’ rift segments? Earth and Planetary Science Letters, v. 297, p. 667–673, doi:10.1016/j.epsl.2010.07.022.

Mortimer, E., Kirstein, L.A., Stuart, F.M., and Strecker, M.R., 2016, Spatio-temporal trends in normal-fault segmentation recorded by low-temperature thermochronology: Livingstone fault scarp, Malawi Rift, East African Rift System: Earth and Planetary Science Letters, v. 455, p. 62–72, doi:10.1016/j.epsl.2016.08.040.

Mortimer, E., Paton, D.A., Scholz, C.A., Strecker, M.R., and Blisniuk, P., 2007, Orthogonal to oblique rifting: effect of rift basin orientation in the evolution of the North basin, Malawi Rift, East Africa: Basin Research, v. 19, p. 393–407, doi:10.1111/j.1365-2117.2007.00332.x.

Muirhead, J.D., and Kattenhorn, S.A., 2018, Activation of preexisting transverse structures in an evolving magmatic rift in East Africa: Journal of Structural Geology, v. 106, p. 1–18, doi:10.1016/j.jsg.2017.11.004.

Muirhead, J.D., Wright, L.J.M., and Scholz, C.A., 2019, Rift evolution in regions of low magma input in East Africa: Earth and Planetary Science Letters, v. 506, p. 332–346, doi:10.1016/j.epsl.2018.11.004.

Nicol, A., Childs, C., Walsh, J.J., Manzocchi, T., and Schöpfer, M.P.J., 2017, Interactions and growth of faults in an outcrop-scale system: Geological Society, London, Special Publications, v. 439, p. 23–39, doi:10.1144/SP439.9.

Nicol, A., Walsh, J., Berryman, K., and Nodder, S., 2005, Growth of a normal fault by the accumulation of slip over millions of years: Journal of Structural Geology, v. 27, p. 327–342, doi:10.1016/j.jsg.2004.09.002.

Ord, D.M., Clemmey, H., and Leeder, M.R., 1988, Interaction between faulting and sedimentation during Dinantian extension of the Solway basin, SW Scotland: Journal - Geological Society (London), v. 145, p. 249–259, doi:10.1144/gsjgs.145.2.0249.

Peacock, D.C.., and Sanderson, D.., 1991, Displacements, segment linkage and relay ramps in normal fault zones: Journal of Structural Geology, v. 13, p. 721–733, doi:10.1016/0191-8141(91)90033-F.

Petersen, M.D. et al., 2015, The 2014 United States National Seismic Hazard Model: Earthquake Spectra, v. 31, p. S1–S30, doi:10.1193/120814EQS210M.

Philippon, M., Willingshofer, E., Sokoutis, D., Corti, G., Sani, F., Bonini, M., and Cloetingh, S., 2015, Slip re-orientation in oblique rifts: Geology, v. 43, p. 147–150, doi:10.1130/G36208.1.

Poirier, J.P., 1980, Shear localization and shear instability in materials in the ductile field: Journal of Structural Geology, v. 2, p. 135–142, doi:10.1016/0191-8141(80)90043-7.

Prater, W.T. et al., 2016, Strain Accomodation of Cenezoic Rifting in the Northern Margin of the Shire Graben, Southern Malawi Rift: American Geophysical Union, Fall Meeting Abstracts,.

Roberts, E.M., Stevens, N.J., O’Connor, P.M., Dirks, P.H.G.M., Gottfried, M.D., Clyde, W.C., Armstrong, R.A., Kemp, A.I.S., and Hemming, S., 2012, Initiation of the western branch of the East African Rift coeval with the eastern branch: Nature Geoscience, v. 5, p. 289–294, doi:10.1038/ngeo1432.

Robertson, E.A.M., Biggs, J., Cashman, K. V., Floyd, M.A., and Vye-Brown, C., 2016, Influence of regional tectonics and pre-existing structures on the formation of elliptical calderas in the Kenyan Rift: Geological Society Special Publication,

v. 420, p. 43–67, doi:10.1144/SP420.12.

Rotevatn, A., Jackson, C.A.L., Tvedt, A.B.M., Bell, R.E., and Blækkan, I., 2019, How do normal faults grow? Journal of Structural Geology, v. 125, p. 174–184, doi:10.1016/j.jsg.2018.08.005.

Rotevatn, A., Kristensen, T.B., Ksienzyk, A.K., Wemmer, K., Henstra, G.A., Midtkandal, I., Grundvåg, S.A., and Andresen, A., 2018, Structural Inheritance and Rapid Rift-Length Establishment in a Multiphase Rift: The East Greenland Rift System and its Caledonian Orogenic Ancestry: Tectonics, v. 37, p. 1858–1875, doi:10.1029/2018TC005018.

Samsu, A., Cruden, A.R., Micklethwaite, S., Grose, L., and Vollgger, S.A., 2020, Scale matters: The influence of structural inheritance on fracture patterns: Journal of Structural Geology, v. 130, p. 103896, doi:10.1016/j.jsg.2019.103896.

Savage, H.M., and Brodsky, E.E., 2011, Collateral damage: Evolution with displacement of fracture distribution and secondary fault strands in fault damage zones: Journal of Geophysical Research, v. 116, p. B03405, doi:10.1029/2010JB007665.

Schlische, R.W., Young, S.S., Ackermann, R. V., and Gupta, A., 1996, Geometry and scaling relations of a population of very small rift-related normal faults: Geology, v. 24, p. 683–686, doi:10.1130/0091-7613(1996)024<0683:GASROA>2.3.CO;2.

Scholz, C.H., Dawers, N.H., Yu, J.Z., Anders, M.H., and Cowie, P.A., 1993, Fault growth and fault scaling laws: preliminary results: Journal of Geophysical Research, v. 98, p. 951–961.

Segall, P., and Pollard, D.D., 1980, Mechanics of discontinuous faults: Journal of Geophysical Research: Solid Earth, v. 85, p. 4337–4350, doi:10.1029/JB085iB08p04337.

Senger, K., Buckley, S.J., Chevallier, L., Fagereng, Å., Galland, O., Kurz, T.H., Ogata, K., Planke, S., and Tveranger, J., 2015, Fracturing of doleritic intrusions and associated contact zones: Implications for fluid flow in volcanic basins: Journal of African Earth Sciences, v. 102, p. 70–85, doi:10.1016/j.jafrearsci.2014.10.019.

Shipton, Z.K., and Cowie, P.A., 2003, A conceptual model for the origin of fault damage zone structures in high-porosity sandstone: Journal of Structural Geology, v. 25, p. 333–344, doi:10.1016/S0191-8141(02)00037-8.

Shipton, Z.K., and Cowie, P.A., 2001, Damage zone and slip-surface evolution over μm to km scales in high-porosity Navajo sandstone, Utah: Journal of Structural Geology, v. 23, p. 1825–1844, doi:10.1016/S0191-8141(01)00035-9.

Smith, M., and Mosley, P., 1993, Crustal heterogeneity and basement influence on the development of the Kenya Rift, East Africa: Tectonics, v. 12, p. 591–606, doi:10.1029/92TC01710.

Stamps, D.S., Saria, E., and Kreemer, C., 2018, A Geodetic Strain Rate Model for the East African Rift System: Scientific Reports, v. 8, p. 1–8, doi:10.1038/s41598-017-19097-w.

Stenvall, C.A., Fagereng, Å., and Diener, J.F.A., 2019, Weaker Than Weakest: On the Strength of Shear Zones: Geophysical Research Letters, v. 46, p. 7404–7413, doi:10.1029/2019GL083388.

Tenthorey, E., and Cox, S.F., 2006, Cohesive strengthening of fault zones during the interseismic period: An experimental study: Journal of Geophysical Research: Solid Earth, v. 111, p. 1–14, doi:10.1029/2005JB004122.

Terzaghi, R.D., 1965, Sources of Error in Joint Surveys: Géotechnique, v. 15, p.

287–304, doi:10.1680/geot.1965.15.3.287.

Torabi, A., and Berg, S.S., 2011, Scaling of fault attributes: A review: Marine and Petroleum Geology, v. 28, p. 1444–1460, doi:10.1016/j.marpetgeo.2011.04.003.

Torabi, A., Johannessen, M.U., and Ellingsen, T.S.S., 2019, Fault Core Thickness: Insights from Siliciclastic and Carbonate Rocks: Geofluids, v. 2019, p. 1–24, doi:10.1155/2019/2918673.

Turcotte, D.L., and Schubert, G., 2002, Geodynamics: New York, Cambridge University Press, 607 p.

Valentini, A., Duross, C.B., Field, E.H., Gold, R.D., Briggs, R.W., Visini, F., and Pace, B., 2019, Relaxing Segmentation on the Wasatch Fault Zone : Impact on Seismic Hazard: v. XX, doi:10.1785/0120190088.

Walker, R.T., Wegmann, K.W., Bayasgalan, A., Carson, R.J., Elliott, J., Fox, M., Nissen, E., Sloan, R.A., Williams, J.M., and Wright, E., 2017, The Egiin Davaa prehistoric rupture, central Mongolia: a large magnitude normal faulting earthquake on a reactivated fault with little cumulative slip located in a slowly deforming intraplate setting: Geological Society, London, Special Publications, v. 432, p. 187–212, doi:10.1144/SP432.4.

Walsh, J.J., Bailey, W.R., Childs, C., Nicol, A., and Bonson, C.G., 2003, Formation of segmented normal faults: A 3-D perspective: Journal of Structural Geology, v. 25, p. 1251–1262, doi:10.1016/S0191-8141(02)00161-X.

Walsh, J.J., Nicol, A., and Childs, C., 2002, An alternative model for the growth of faults: Journal of Structural Geology, v. 24, p. 1669–1675, doi:10.1016/S0191-8141(01)00165-1.

Walters, R.J. et al., 2018, Dual control of fault intersections on stop-start rupture in the 2016 Central Italy seismic sequence: Earth and Planetary Science Letters,

v. 500, p. 1–14, doi:10.1016/j.epsl.2018.07.043.

Wästeby, N., Skelton, A., Tollefsen, E., Andrén, M., Stockmann, G., Claesson Liljedahl, L., Sturkell, E., and Mörth, M., 2014, Hydrochemical monitoring, petrological observation, and geochemical modeling of fault healing after an earthquake: Journal of Geophysical Research: Solid Earth, v. 119, p. 5727–5740, doi:10.1002/2013JB010715.

Watterson, J., 1975, Mechanism for the persistence of tectonic lineaments: Nature, v. 253, p. 520–522, doi:10.1038/253520b0.

Wedmore, L.N.J., Biggs, J., Williams, J.N., Fagereng, Å., Dulanya, Z., Mphepo, F., and Mdala, H., 2019, Active fault scarps in southern Malawi and their implications for the distributino and evolution of strain in amagmatic continental rifts: EarthArXiv, doi:10.31223/osf.io/ujchx.

Wei, S. et al., 2011, Superficial simplicity of the 2010 El Mayor–Cucapah earthquake of Baja California in Mexico: Nature Geoscience, v. 4, p. 615–618, doi:10.1038/ngeo1213.

Wesnousky, S.G., 2008, Displacement and geometrical characteristics of earthquake surface ruptures: Issues and implications for seismic-hazard analysis and the process of earthquake rupture: Bulletin of the Seismological Society of America, v. 98, p. 1609–1632, doi:10.1785/0120070111.

Wesnousky, S.G., 2006, Predicting the endpoints of earthquake ruptures: Nature, v. 444, p. 358–360, doi:10.1038/nature05275.

Westerhof, A.P., Lehtonen, M.I., Mäkitie, H., Manninen, T., Pekkala, Y., Gustafsson, B., and Tahon, A., 2008, The Tete-Chipata Belt: a new multiple terrane element from western Mozambique and southern Zambia: Geological Survey of Finland Special PAper, v. 48, p. 145–166.

Wheeler, W.H., and Karson, J.A., 1989, Structure and kinematics of the Livingstone Mountains border fault zone, Nyasa (Malawi) Rift, southwestern Tanzania: Journal of African Earth Sciences (and the Middle East), v. 8, p. 393–413, doi:10.1016/S0899-5362(89)80034-X.

Whipp, P.S., Jackson, C.A.L., Gawthorpe, R.L., Dreyer, T., and Quinn, D., 2014, Normal fault array evolution above a reactivated rift fabric; a subsurface example from the northern Horda Platform, Norwegian North Sea: Basin Research, v. 26, p. 523–549, doi:10.1111/bre.12050.

Willemse, E.J.M., 1997, Segmented normal faults: Correspondence between three-dimensional mechanical models and field data: Journal of Geophysical Research: Solid Earth, v. 102, p. 675–692, doi:10.1029/96jb01651.

Willemse, E.J.M., Pollard, D.D., and Aydin, A., 1996, Three-dimensional analyses of slip distributions on normal fault arrays with consequences for fault scaling: Journal of Structural Geology, v. 18, p. 295–309, doi:10.1016/S0191-8141(96)80051-4.

Williams, J.N., Fagereng, Å., Wedmore, L.N.J., Biggs, J., Mphepo, F., Dulanya, Z., Mdala, H., and Blenkinsop, T., 2019, How Do Variably Striking Faults Reactivate During Rifting? Insights From Southern Malawi: Geochemistry, Geophysics, Geosystems, p. 3588–3607, doi:10.1029/2019gc008219.

Williams, J.N., Toy, V.G., Smith, S.A.F., and Boulton, C., 2017, Fracturing, fluid-rock interaction and mineralisation during the seismic cycle along the Alpine Fault: Journal of Structural Geology, v. 103, p. 151–166, doi:10.1016/j.jsg.2017.09.011.

Wilson, J.., Chester, J.., and Chester, F.., 2003, Microfracture analysis of fault growth and wear processes, Punchbowl Fault, San Andreas system, California:

Journal of Structural Geology, v. 25, p. 1855–1873, doi:10.1016/S0191-8141(03)00036-1.

Woolley, A.R., 1987, Lithosphere metasomatism and the petrogenesis of the Chilwa Province of alkaline igneous rocks and carbonatites, Malawi: Journal of African Earth Sciences, v. 6, p. 891–898, doi:10.1016/0899-5362(87)90048-0.

Woolley, A.R., Bevan, J.C., and Elliott, C.J., 1979, The Karroo dolerites of southern Malawi and their regional geochemical implications: Mineralogical Magazine, v. 43, p. 487–495, doi:10.1180/minmag.1979.043.328.08.

Worthington, R.P., and Walsh, J.J., 2017, Timing, growth and structure of a reactivated basin-bounding fault: Geological Society, London, Special Publications, v. 439, p. 511–531, doi:10.1144/SP439.14.

Zangerl, C., Loew, S., and Eberhardt, E., 2006, Structure, geometry and formation of brittle discontinuities in anisotropic crystalline rocks of the Central Gotthard Massif, Switzerland: Eclogae Geologicae Helvetiae, v. 99, p. 271–290, doi:10.1007/s00015-006-1190-0.

Zeeb, C., Gomez-Rivas, E., Bons, P.D., and Blum, P., 2013, Evaluation of sampling methods for fracture network characterization using outcrops: AAPG Bulletin, v. 97, p. 1545–1566, doi:10.1306/02131312042.

Zhang, P., Slemmons, D.B., and Mao, F., 1991, Geometric pattern, rupture termination and fault segmentation of the Dixie Valley-Pleasant Valley active normal fault system, Nevada, U.S.A.: Journal of Structural Geology, v. 13, p. 165–176, doi:10.1016/0191-8141(91)90064-P.

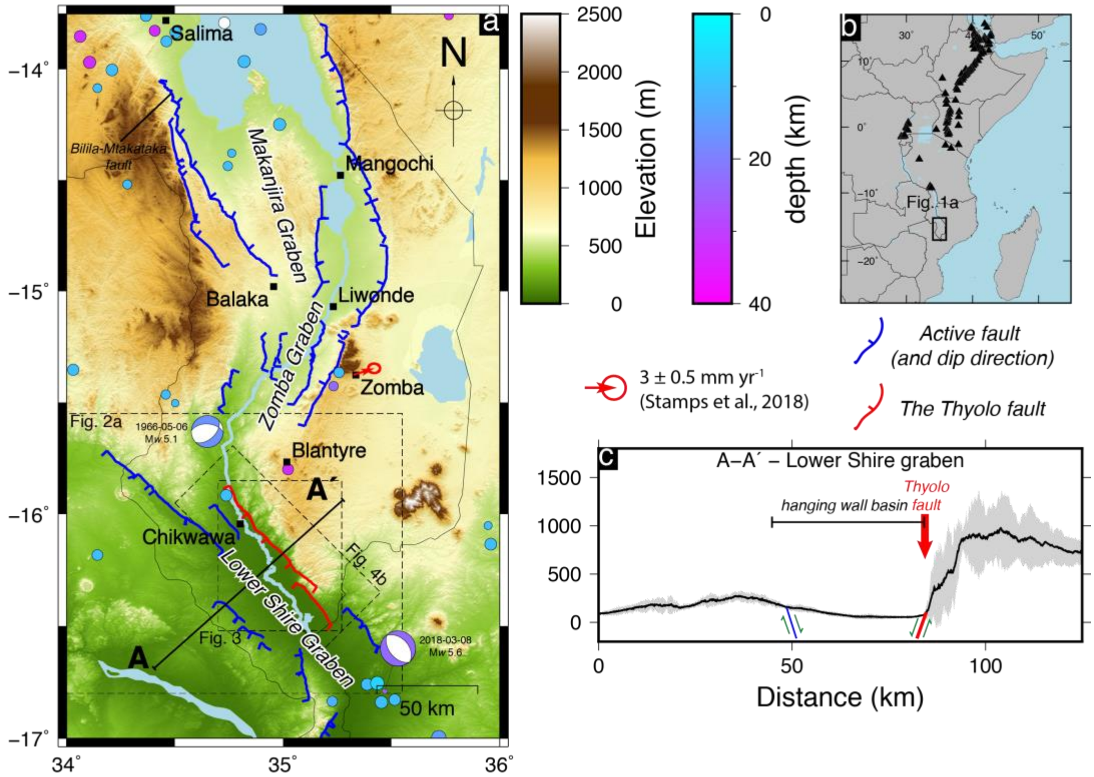

Figure 1. The location and tectonic context of the Lower Shire Graben. (a) The southern Malawi rift system with known active fault scarps in blue and the Thyolo fault highlighted in red. Also shown is the GPS vector from a station in Zomba, National Earthquake Information Centre earthquake locations from 1971-2018 (circles coloured by depth), and focal mechanisms for the two largest events in the region, a M*w*5.1 earthquake in 1966 (from Craig et al., 2011) and the CMT solution for the 2018 Nsanje earthquake (M*w*5.6). (b) The location of the southern Malawi rift system within the East African Rift. Triangles indicate Holocene active volcanoes. (c) Swath topographic cross section across the Lower Shire Graben extracted from TanDEM-X data. Black line is the median elevation with the grey shading the maximum and minimum elevation 10 km either side of profile A-A` indicated in part a.

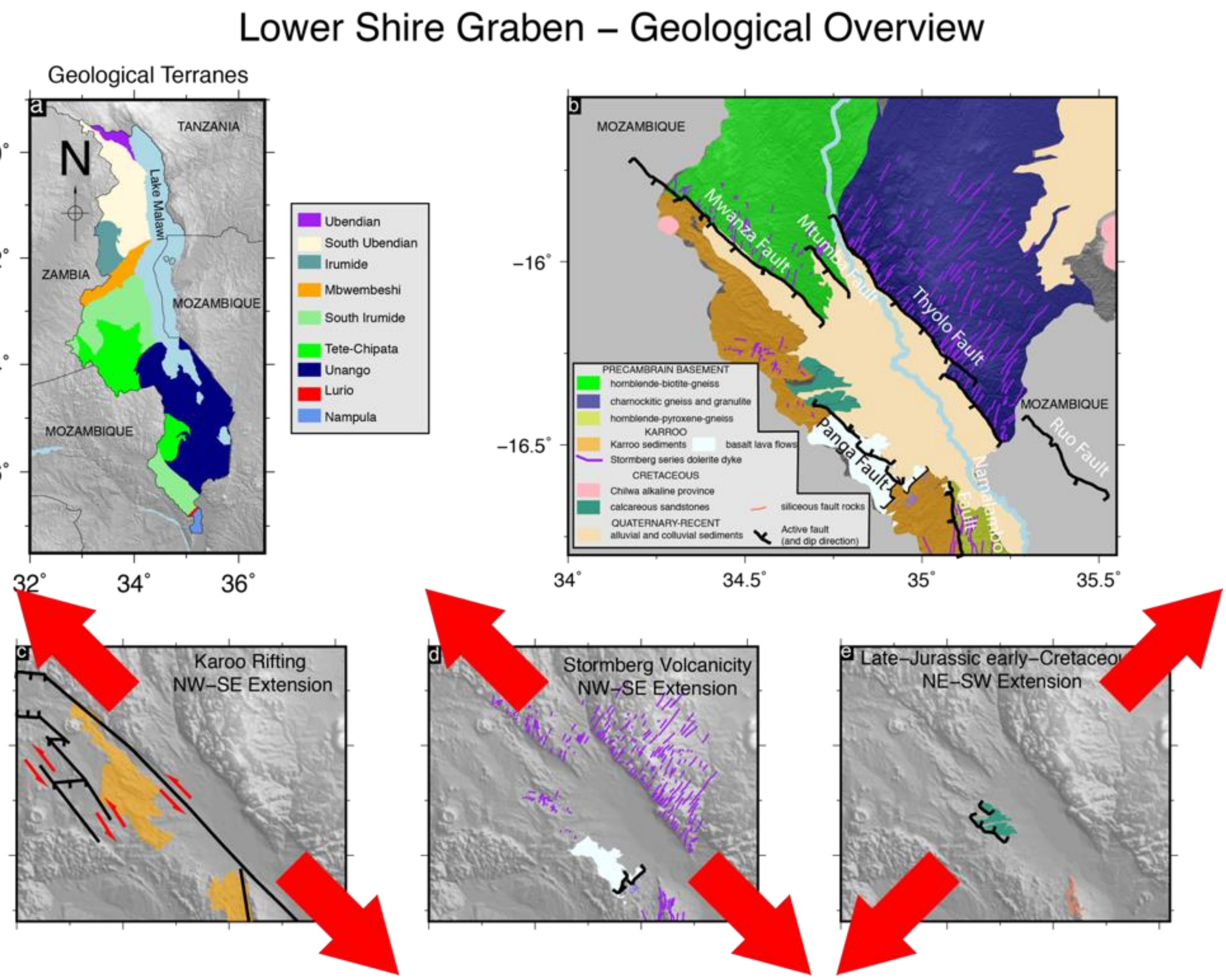

Figure 2. Geological overview of the Lower Shire Graben. (a) Geological terranes within Malawi (Fullgraf et al., *in press*). (b) Simplified geological map of the Lower Shire Graben adapted from Hapgood 1963. (c) Structures related to NW-SE amagmatic extension during the Karoo period. (d) Dykes and normal faults associated with NW-SE magmatic rifting in the late Karoo period. (e) Normal faults and sedimentary deposits related to NE-SW rifting during the Late-Jurassic to early-Cretaceous.

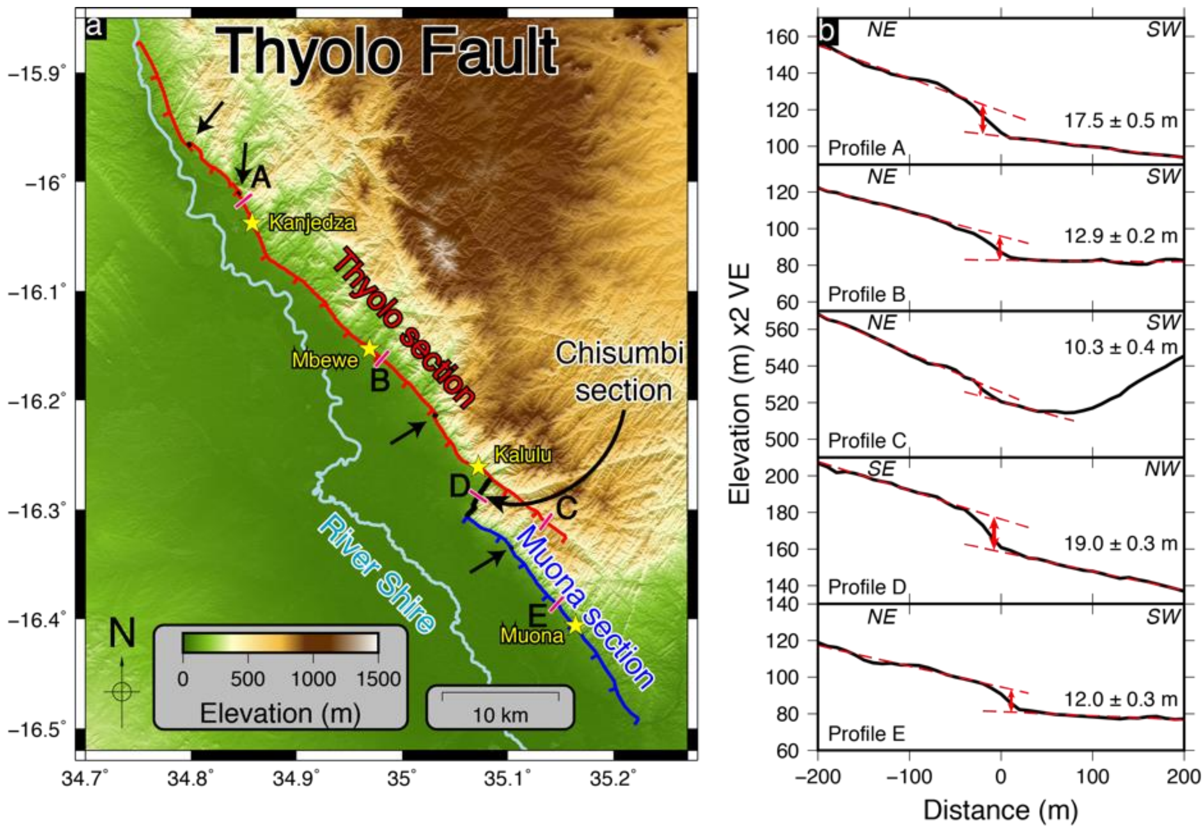

Figure 3 (a) TanDEM-X digital elevation model of the Thyolo fault showing both the Thyolo (red) and Muona (blue) sections. The fault sections oriented at ~90° to the main strike are indicated in black with sections visible at this scale identified by black arrows . Yellow stars indicate the locations of field studies reported in this paper. Pink rectangles indicate are the locations and orientation of illustrative topographic profiles extracted perpendicular to the fault scarp and shown in part b. (b) Example topographic profiles extracted perpendicular the fault scarp. All profiles are plotted with the footwall on the left-hand side (profile orientation is indicated in the top left). Note profile D is located along the Chisumbi section where the strike is oriented ~90° to the strike of the main fault sections.

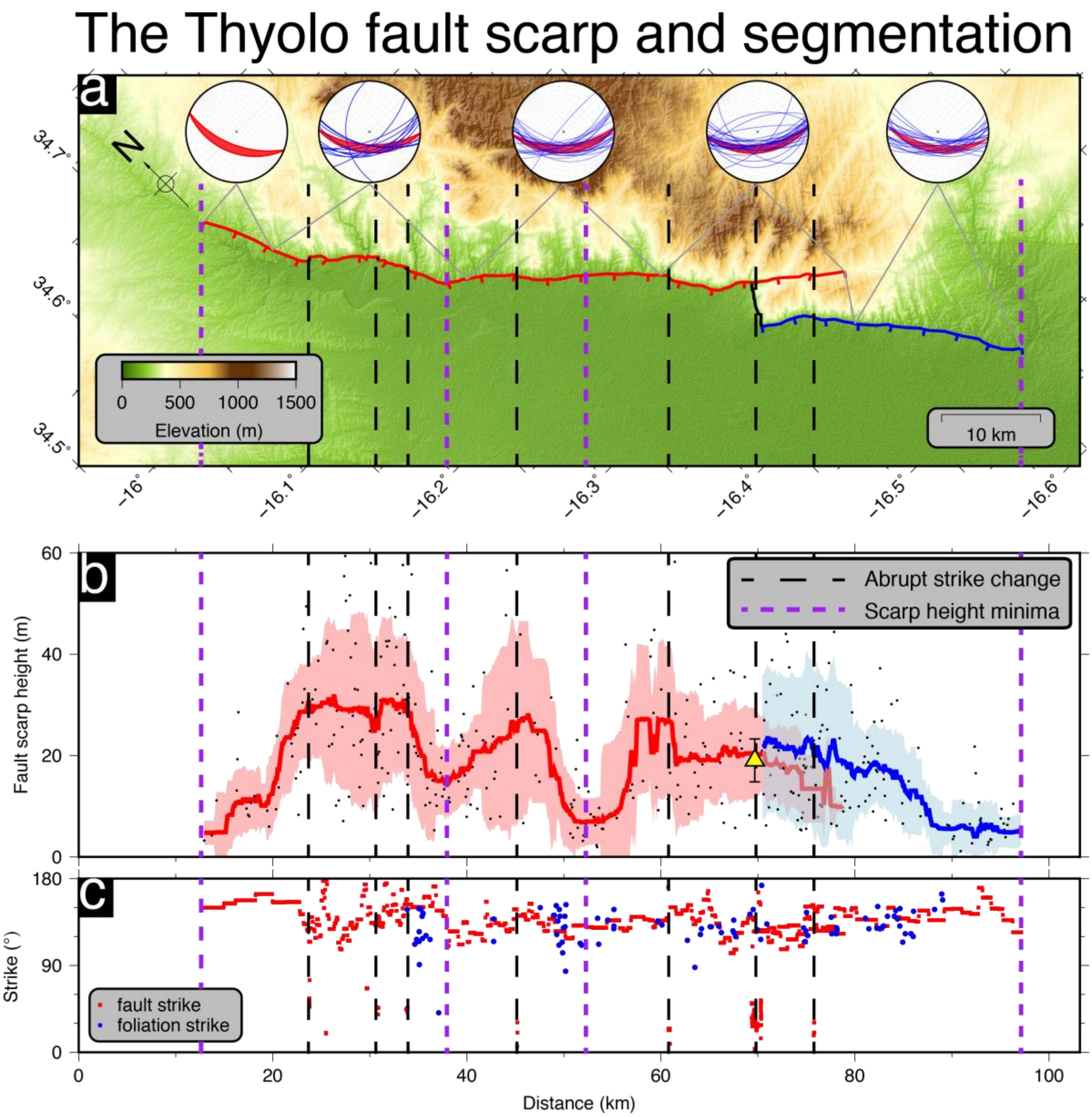

Figure 4. Thyolo fault scarp height and segmentation. (a) A rotated view of the Thyolo fault showing different indicators of fault segmentation. Inset equal angle, lower hemisphere stereonets are rotated into the same view as the underlying map. Red ellipses shows the mean fault orientation measured every 20 km, with a dip value plotted between 45°-60°, and the blue lines show foliation orientations. (b) The height of the Thyolo fault scarp as a function of distance from the NW to the SE along the fault. (c) The strike of the Thyolo fault (measured every 50 m) and foliation strike measurements (Habgood et al., 1973) as a function of distance from NW to SE

along the fault. Scarp height in b was measured using topographic profiles, perpendicular to the scarp, extracted every 100 m along strike. Black dots are the individual measurements with the solid coloured lines the 5 km moving median of these measurements. The shaded areas represents the 1σ error bars. Red line is the Thyolo section, blue line is the Muona section. The yellow triangle (with 1σ error bars) is the scarp height along the ~4 km linking segment.

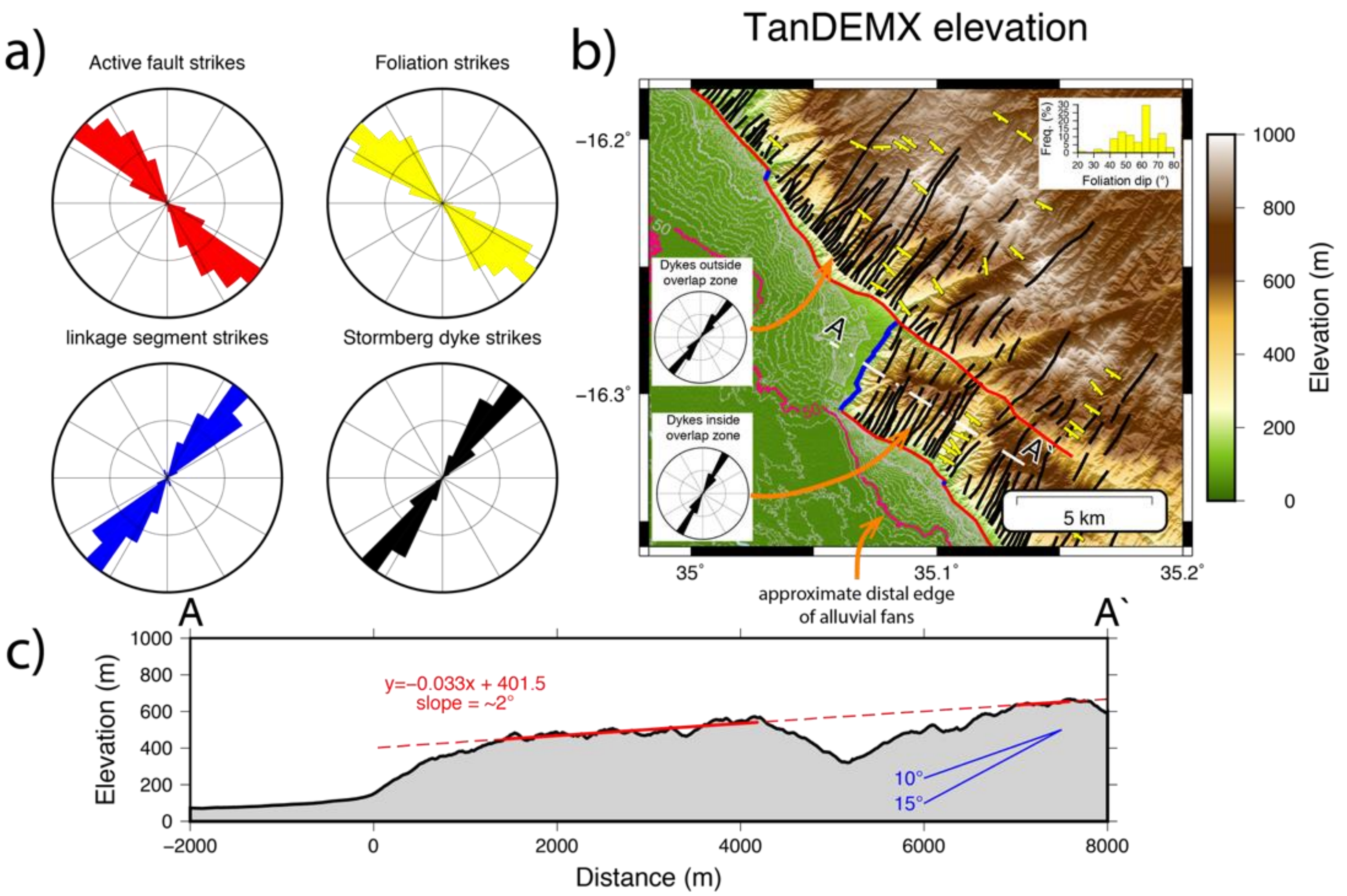

Figure 5. The linkage section between the Thyolo and Muona sections. (a) Rose diagrams of the orientation of surface traces of the different structures along the Thyolo fault. Active faults include the Thyolo and Muona fault sections as indicated on the map. The fault sections and dykes were divided into 50 m long sections before calculating the strike of each section. Linkage segments only include the sections of fault that strike approximately perpendicular to the Thyolo and Muona sections. Foliation orientations and Stormberg dykes were digitised from Habgood et al. (1973). (b) TanDEM-X DEM of the Chisumbi linkage section between the Thyolo and Muona sections. Dykes are indicated with black lines, foliation orientation and dip direction with yellow lines and ticks, faults with red lines and sections of the fault that strike perpendicular to the main fault with blue lines. Grey contour lines are 2.5 m apart, with the 50 m contour, which marks the approximate distal edge of alluvial fan complexes originating from footwall catchments, marked in pink. The inset

histogram shows the dip of foliation measurements (Habgood et al., 1973). The inset rose diagrams show the orientation of dykes located inside and outside of the zone where the Thyolo and Muona sections overlap. (c) Swath topographic extracted along the transect A-A` shown in part b. The mean topography 1 km either side of the transect is plotted. The red line is a linear best fit to the slope of the topography within the portions of the solid red line. The dashed portions are not used as they have been affected by erosion due to river incision or include the fault scarp and fault facet slope. Angles which are the normal range of breached relay ramp dips (according to Fossen and Rotevatn, 2016) are plotted for comparison.

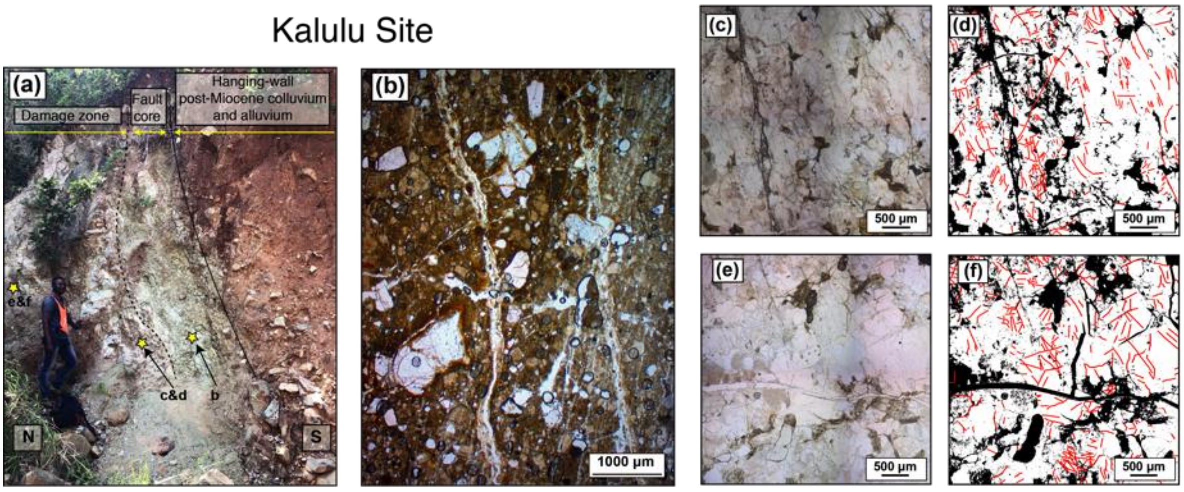

Figure 6 (a) Fault zone exposure at Kalulu showing juxtaposition of hanging wall sediments and footwall basement across a 0.7 m unit of fault gouge. Locations of samples used for photomicrographs in (b-f) shown by yellow stars. (b) photomicrograph of gouge with fractured quartz clasts and clay-rich brown matrix in plane polarised light (PPL) in sample from fault contact. (c-f) Photomicrographs of samples in PPL with adjacent image showing fracture traces (red lines) and areas (black) in sample not constituting quartz or feldspar grains that were omitted when calculating fracture density.

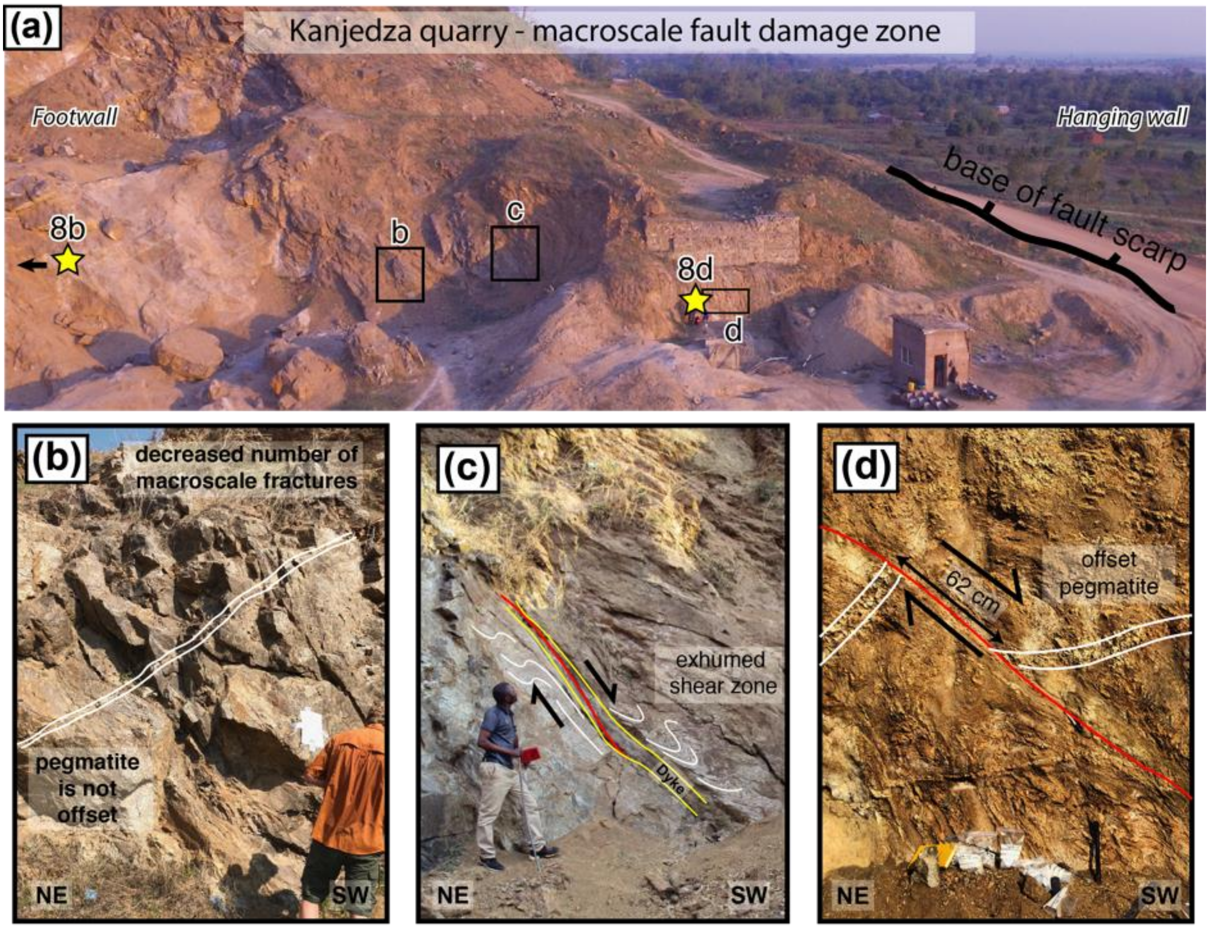

Figure 7. Macroscale fault damage zone at the Kanjedza site along the Thyolo fault. (a) A perspective view of the exposed fault zone indicating the location of sample macroscale photos shown in parts b-d. Locations of microscale observations shown in Figure 8 are indicated with yellow stars. (b) Outcrop from outside the macroscale fault damage zone, note the lack of fracturing within the basement rock when compared with c and d. (c) Outcrop within the fault damage zone showing an exhumed reverse sense shear zone and dyke. The dyke edge has been reactivated in a normal sense and acts as a minor slip surface. (d) Offset pegmatite within the footwall damage zone.

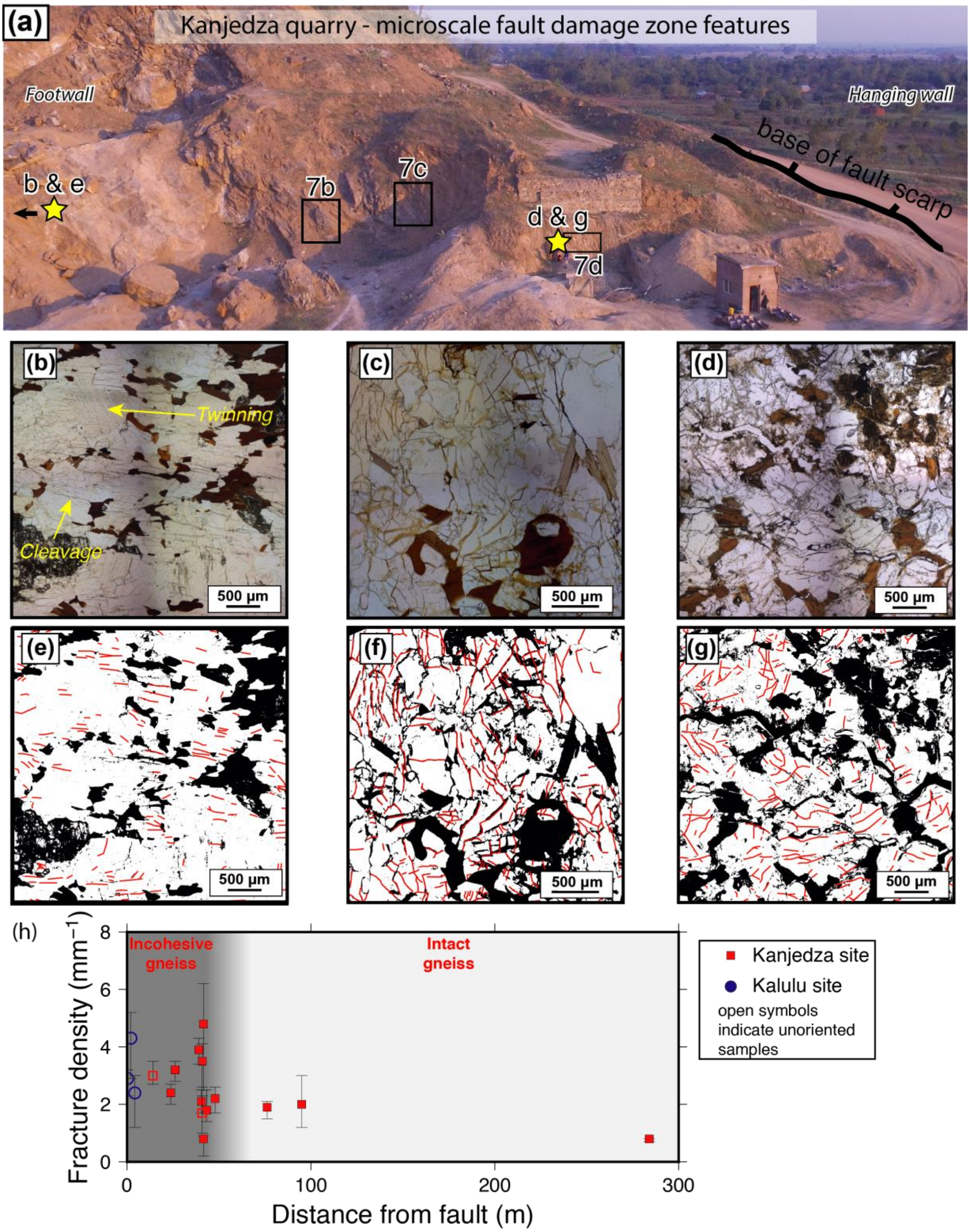

Figure 8. Microscale fault damage zone at Kanjedza Quarry. (a) An overview of the Kanjedza quarry fault zone exposure indicating the locations of the samples (yellow stars). (b) Photomicrograph of sample from outside the fault zone. (c)

Photomicrograph of a sample from a minor footwall slip surface. (d) Photomicrograph of a sample in the fault damage zone surrounding minor footwall fault and dyke (e-f) annotated photomicrographs of parts b-g showing the fractures (red lines) identified in each sample. (h) Compilation of fracture density plotted against distance from the fault for the Kanjedza and Kalulu sites along the Thyolo fault. The division between intact and incohesive gneiss is based on field observations (Figure 7).

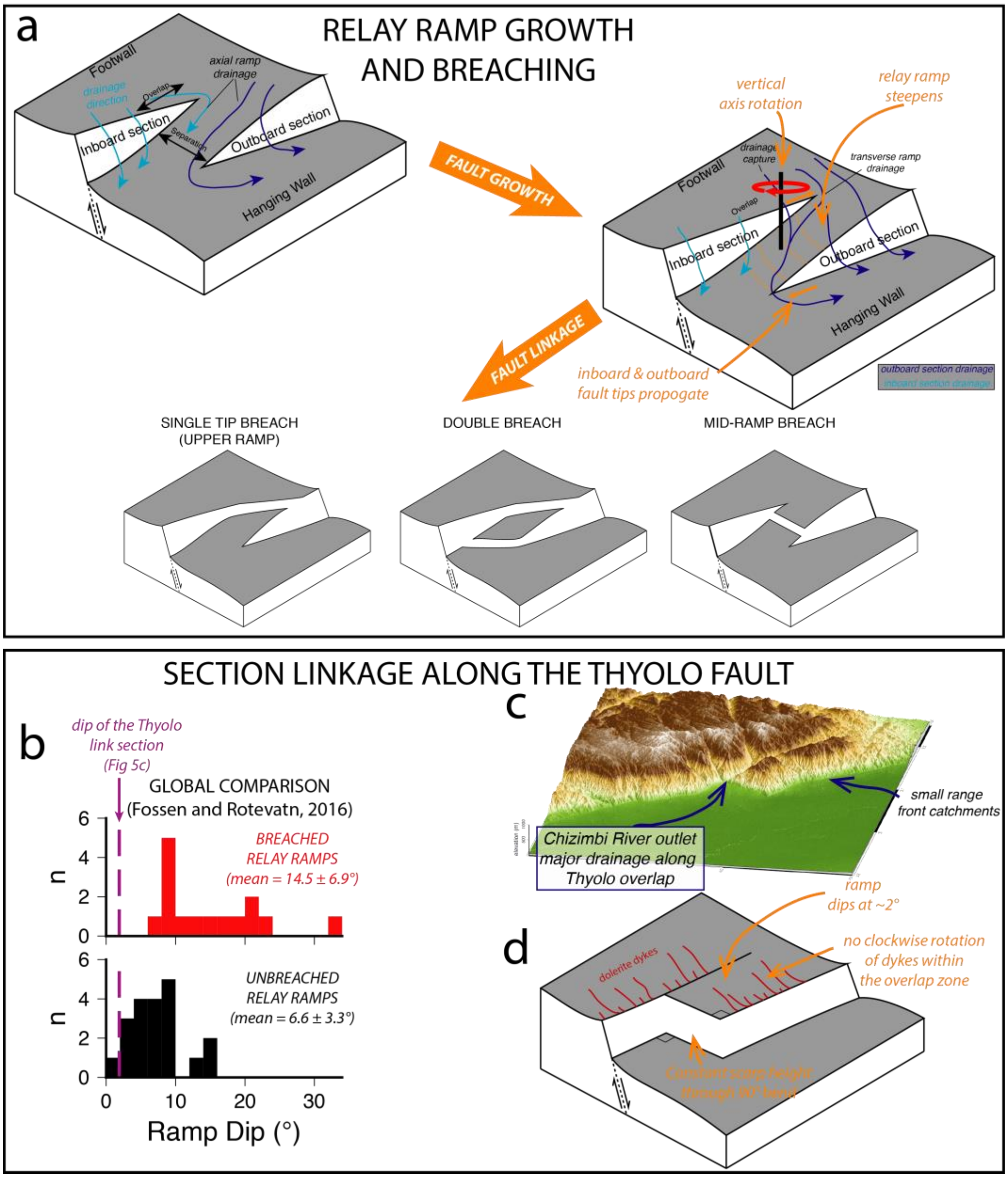

Figure 9. A comparison of relay ramp morphology and the linkage section between the Thyolo and Muona sections. (a) A summary of relay ramp growth and breaching (adapted from Fossen and Rotevatn, 2016). (b) The dip of relay ramp dips from a global compilation of breached and unbreached relay ramps (Fossen and Rotevatn, 2016). The dip of the topography in the section between the Thyolo and Muona sections is indicated with the purple dashed line. (c) A 3d view of the link section between the Thyolo and Muona sections showing the prominent drainage channels including the range front catchments that are predominate in the region and the

triangular facets along the Chisumbi section. (d) A conceptual view of the way the Thyolo fault has linked between the Thyolo and Muona sections.

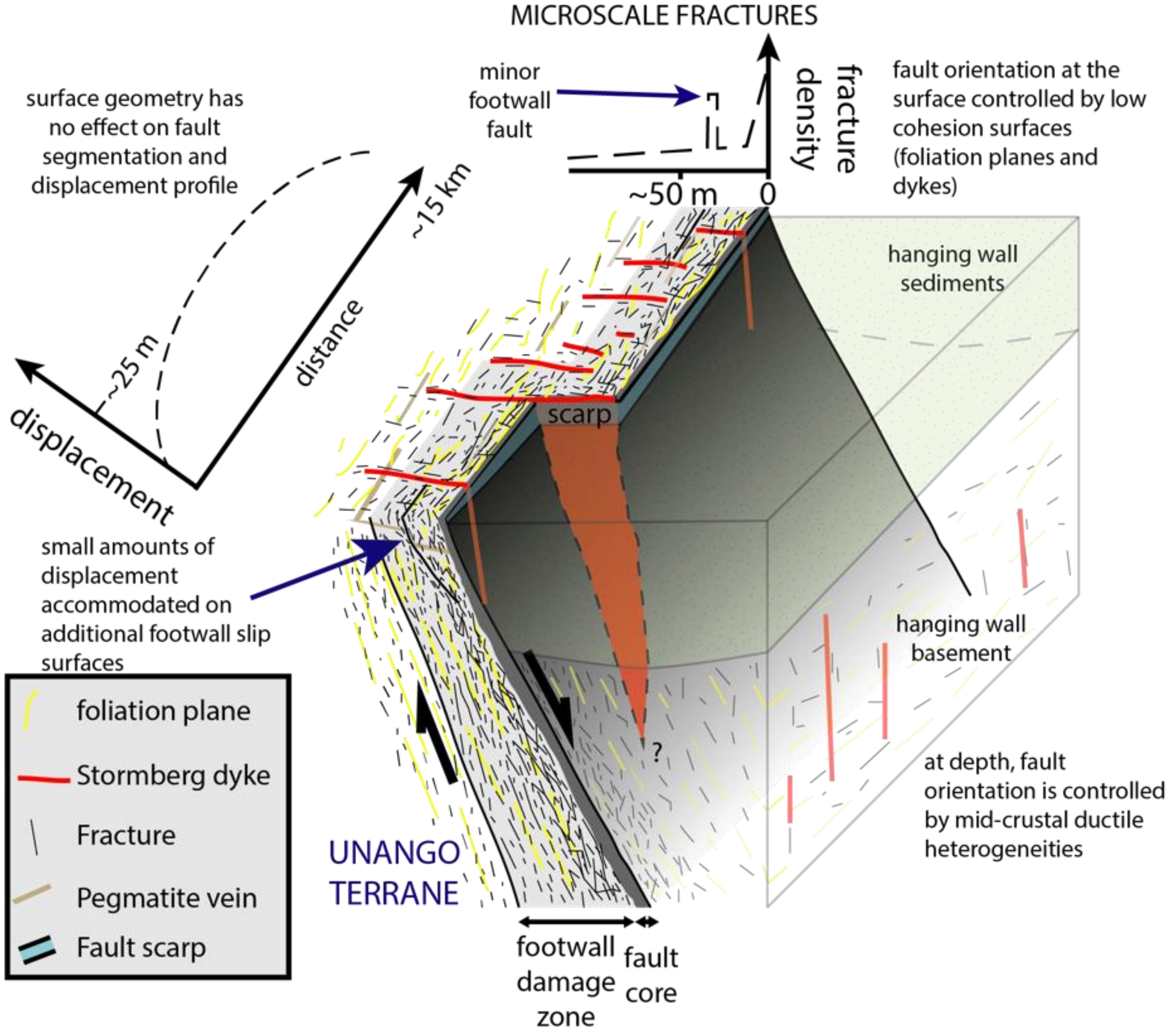

Figure 10. A conceptual model of the reactivation of the Thyolo fault towards the edge of the Unango Terrane boundary showing the relationship between shallow brittle structures which control the small scale surface geometry and fault damage zone structure, and deeper mid-crustal ductile, viscous structures associated with the terrane boundary which control the overall geometry of the fault and possibly the pattern of segmentation.